

Local calibration of verbal autopsy algorithms

Abhirup Datta

Department of Biostatistics, Johns Hopkins University

and

Jacob Fiksel

Department of Biostatistics, Johns Hopkins University

and

Agbessi Amouzou

Department of International Health, Johns Hopkins University

and

Scott Zeger

Department of Biostatistics, Johns Hopkins University

May 30, 2022

Abstract

Computer coded verbal autopsy (CCVA) algorithms are commonly used to generate burden of disease estimates using data from verbal autopsy surveys in low and middle income countries with poor vital registration data on causes of death. In settings where local training data is scarce, CCVA algorithms typically rely on some non-local gold standard training data and may yield inaccurate estimates in local context. We present a general calibration framework to improve estimates of cause specific mortality fractions from CCVA algorithms when a limited amount of local training data is available. We formulate a Bayesian hierarchical model for local calibration of discrete classifiers that updates a non-locally trained CCVA estimate using estimates of the misclassification rates of the CCVA algorithm on the local training data. Our approach involves a novel transition matrix shrinkage for the misclassification matrix. We demonstrate theoretically how this regularization guarantees that, in absence of any local data or when the CCVA algorithm classifies perfectly on the local training data, the calibrated estimate coincides with the naive estimate of prevalence, thereby subsuming the default estimation procedure as a special case of our approach. We present a novel Gibbs

sampler using data augmentation that enables fast implementation. Our calibration is agnostic to the choice of CCVA algorithm and hence can leverage the output from any of the publicly available CCVA software. Since, there are many available CCVA algorithms and in practice we do not know which one will be more accurate, we also present an ensemble Bayesian calibration approach that uses predictions from multiple CCVA algorithms as inputs to produce an unified estimate of prevalence. We present a theoretical result demonstrating how the ensemble calibration favors the most accurate algorithm and robustifies the estimation. Simulation studies and analysis of the PHMRC data reveals that the calibrated estimates are more accurate than their uncalibrated analogs, and that the ensemble calibration generally agrees with the best performing CCVA algorithm. We also present extensions to model the etiology distribution as functions of demographic covariates, and an EM algorithm based MAP estimation as an alternate to MCMC. We have created an R-package which implements this calibration method and is available on Github.

Keywords: Bayesian, Cause of death, Calibration, Gibbs sampler, Hierarchical modeling, Regularization, Verbal Autopsy

1 Introduction

In low and middle income countries, it is infeasible to conduct full autopsies for the majority of deaths due to economic, human resource, and infrastructural constraints, and/or religious or cultural prohibitions against autopsies (AbouZahr et al. 2015, Allotey et al. 2015). An alternative method to infer the cause (or "etiology") of death (COD) is to conduct *verbal autopsy* (VA) – a systematic interview of the relatives of the deceased individual to obtain information about symptoms observed prior to death (Soleman et al. 2006). The reported symptoms in the VA can then be assessed by a group of physicians who assign the likely cause(s) of death. COD data derived from VAs can subsequently be aggregated into cause-specific mortality rates, that can in turn guide public health policy.

While *physician coded* VA is a useful alternative to full autopsies, scaling the process to the regional or national level is challenging. Consequently, over the last decade several data-driven solutions have been proposed that replace the physician coding with artificial

intelligence software. These *computer coded* VA (CCVA) algorithms predict COD using the VA records as input. Examples include Tariff (James et al. 2011, Serina et al. 2015), interVA (Byass et al. 2012), insilicoVA (McCormick et al. 2016), the King and Lu method (King et al. 2008), as well as software implementation of the medical decision process adopted by physicians in determining COD (expert algorithm, Kalter et al. 2015). The ease of use and scalability of CCVA algorithms has led to their rapid gain in popularity, including being now recommended by World Health Organization (Nichols et al. 2018).

Formally, the task of estimating cause-specific mortality fractions (CSMF) can be decomposed as $P(c) = \int P(c | \mathbf{s}) dP(\mathbf{s})$ where c is a cause and the VA record \mathbf{s} is a list of symptoms. A countrywide VA survey only provides information about the marginal distribution of the symptoms $P(\mathbf{s})$. Learning the mapping $P(c | \mathbf{s})$ requires *gold standard* (GS) information – either from a training dataset containing true COD information alongside the corresponding symptoms, obtained locally or from past surveys in other countries, or some standard symptom-given-cause propensity matrix. Even with training data, estimating $P(c | \mathbf{s})$ is challenging as the symptom space is high-dimensional, typically a few hundred symptoms.

This manuscript addresses the situation where VA records are available for a representative subset of the entire population but gold standard cause of death (GS-COD) data are ascertained for only a very small fraction of these deaths. Nationally representative VA surveys like the **Countrywide Mortality Surveillance for Action (COMSA)** in Mozambique and in Sierra Leone (references) typify this circumstance. Due to the unavailability of local GS data, CCVA algorithms are trained on non-local GS data to estimate the population mortality rates attributable to each of the causes as well as variations in the rates in space and time. For example, the publicly available Population Health Metrics Research Consortium (PHMRC) Gold Standard VA database (CJL et al. 2011), which has more than 10,000 paired physician and VA assessments of cause of death across 4 countries, is often leveraged to train the CCVA algorithms. With such a large gold-standard data set, estimates of

$P(c \mid \mathbf{s})$ are highly precise. However, there exists considerable skepticism about the utility of CCVA trained on non-local data. Past studies have shown how using training data collected non-locally tends to sacrifice accuracy for precision (McCormick et al. 2016). Similarly, use of a default propensity matrix, based on knowledge not specific to the country of interest, has also been shown to introduce substantial bias (Flaxman et al. 2018).

Our solution to this bias – variance trade-off problem is to use non-local gold-standard data to obtain an initial prediction, but to refine it with local gold standard data. We proffer a general calibration framework for obtaining population CSMF estimates in a new country using countrywide VA records and a limited amount of local GS data with the true COD. Our calibration approach is to first use one or more CCVA algorithms trained on non-local GS information, then use limited local GS data to update the initial CSMF to arrive at an improved final estimate.

With C causes and S -dimensional symptoms, the advantage of this new approach is that the limited GS data for the new country is only used to estimate the $C \times C$ matrix of the misclassification rates instead of the SC parameters needed to train a CCVA algorithm in the first place. Since $S \gg C$ this considerably reduces the dimensionality of the problem. To ensure a stable estimation of the misclassification matrix, we additionally use a regularization prior that shrinks the misclassification matrix towards identity. The prior ensures that the CSMF estimate from the calibration model is shrunk towards the CSMF estimate from the CCVA algorithm unless there is substantial disagreement between the CCVA predicted COD and the true COD in the local GS data. We establish the theoretical guarantee that in absence of any local GS data or in the case of perfect agreement between the CCVA and the true COD in the local GS data, our calibration approach does not alter the CSMF estimate from the CCVA, thereby showing that the naive application of CCVA is a special case of our algorithm. A novel Gibbs sampler scheme with augmented data is devised for fast implementation of the Bayesian hierarchical calibration model. Our calibration algorithm

also gives individual COD predictions although it is not the primary goal in COMSA.

Our algorithm is completely agnostic to the choice of the CCVA algorithm; it only uses its COD predictions. Hence, we can leverage one or more publicly available algorithms to obtain the predictions and subsequently perform the calibration in the low-dimensional prediction (cause) space. Simulation and data analyses reveal that for all scenarios considered, estimation of CSMF from our calibration model can be considerably improved over the raw estimate from input CCVA algorithm(s).

There exists considerable disagreement about which CCVA algorithm is the most accurate (Leitao et al. 2014, McCormick et al. 2016, Flaxman et al. 2018). In our experience, no method is universally superior. Since it is not possible to a priori choose the most accurate CCVA algorithm, we also propose an ensemble calibration approach that uses as input predictions from multiple CCVA algorithms. The ensemble calibration accomplishes method-averaging over different CCVA algorithms to reduce the risk of using a CCVA approach that is inferior to others in a particular study. We establish a theoretical result that the CSMF estimate of the ensemble model coincides with that from a CCVA algorithm which offers perfect accuracy on the local GS dataset. A Gibbs sampler for the ensemble calibration is also developed, as well as a computationally lighter version of the model that is much faster and involves fewer parameters. Simulation and data analyses demonstrate how the ensemble sampler consistently produces CSMF estimates similar to those produced by using the calibration approach on the best CCVA algorithm.

The rest of the manuscript is organized as follows. In Section 2, we introduce notation and state the statistical problem precisely. In Sections 3 and 4, we present the calibration methodology and its extension to the ensemble case. Section 5 presents simulation results. Section 6 returns to the motivating dataset with an analysis of the PHMRC data. Section 7 presents an EM algorithm approach to obtain maximum a posteriori (MAP) estimates for the calibration model, as a fast alternative to the fully Bayesian approach adopted earlier.

Section 8 considers the extension where CSMF can be modeled as a function of covariates like age and sex, and spatial regions. We end the manuscript in Section 9 with a discussion of limitations and future research opportunities. A glossary of acronyms used throughout the manuscript is provided in Table 1.

Acronym	Full form	Acronym	Full form
VA	Verbal autopsy	PHMRC	Population Health Metrics Research Consortium
CCVA	Computer coded VA	COMSA	Countrywide Mortality Surveillance for Action
COD	Cause of Death	CSMF	Cause Specific Mortality Fraction
CSMFA	CSMF accuracy	GS-COD	Gold-standard Cause of Death
CCC	Chance corrected concordance	MIA	Minimally Invasive Autopsy

Table 1: Glossary of acronyms used in the manuscript

2 Setup

Let A denote a generic CCVA algorithm, i.e., a function from the space of S dimensional symptoms to the categorical space of C mutually exclusive causes. The CSMF are typically available either as a direct output of A , or can be calculated indirectly by dividing the predicted number of individuals with a specific cause by the total number of deaths. Broadly speaking, inputs to A include some gold standard information \mathcal{G} , needed to learn the probabilities $P(c \mid \mathbf{s})$ for any cause-symptom pair, and, to calculate population CSMFs, a *population set* \mathcal{P} consisting of only VA records for thousands of individuals collected via a countrywide survey. CCVA methods like Tariff and the approach in King et al. (2008) represent a traditional supervised learning approach, where \mathcal{G} is a substantial training dataset, constituting paired VA records and gold standard COD (GS-COD) from full autopsy or physician’s opinion. InterVA is a semi-supervised learning approach where a standard matrix of letter grades representing the propensity of each symptom given each cause is used

as the gold standard information \mathcal{G} . InsilicoVA generalizes InterVA and endows the problem with a proper probabilistic framework allowing coherent statistical inference. It adapts to the type of gold standard input and can work with either the default symptom-cause matrix used in InterVA or estimate this matrix based on some gold standard training data of paired VA and GS-COD records.

As discussed earlier, past studies reveal that CCVA algorithms are most accurate when \mathcal{G} is a local training dataset with paired VA records and true COD. This manuscript focuses on the setting where although a large population set \mathcal{P} is available, true COD has been determined for a smaller fraction of these deaths. This reflects the objectives set by the ongoing COMSA projects in Mozambique and Sierra Leone where, in addition to conducting a nationally representative VA survey which yields \mathcal{P} , researchers will collect GS-COD for a small number of deaths from one or two local hospitals in each country that perform minimally invasive autopsies (MIA) (Byass 2016). Pairing the COD information from full or minimally invasive autopsies in the hospital to the respective VA records will create a small local gold standard dataset. We refer to this as the hospital set \mathcal{H} . Budgetary constraints and socio-cultural factors unfortunately imply that only a handful of deaths can eventually be autopsied (up to a few hundred).

The VA report usually consists of responses to about $S = 100$ to 250 questions. It is challenging to learn the $c \mid \mathbf{s}$ relationships owing to this high-dimensionality of the symptom space. Even if the responses are dichotomized, assuming S symptoms and C causes, $P(c \mid \mathbf{s})$ is a mapping from the symptom (covariate) space $\{0, 1\}^S \rightarrow \mathcal{S}^C$ where \mathcal{S}^C denotes the simplex space of discrete probability distributions with C support points, i.e., $\mathcal{S}^C = \{(\pi_1, \pi_2, \dots, \pi_c) \mid \pi_i \geq 0, \sum_{i=1}^C \pi_i = 1\}$. Hence, the hospital set \mathcal{H} with limited sample size falls well short of adequacy for directly serving as the gold standard information \mathcal{G} for these complex CCVA algorithms.

Since the VA questionnaire has now been standardized by the World Health Organization

(WHO), borrowing strength from a large training data of VA surveys and gold standard COD collected previously in other countries is becoming increasingly customary for VA studies in new countries. Alternatively, one can also use InterVA or InsilicoVA as the CCVA algorithm with \mathcal{G} being the default $P(s | c)$ matrix. Either choices of \mathcal{G} represent information collected in countries different from the country of interest and hence may possibly engender biases in CSMF estimates from A . Perhaps a slightly better alternative would be to append the existing training data \mathcal{G} from other countries with the local training data \mathcal{H} . However, results may not change substantially, as \mathcal{H} is far outnumbered by \mathcal{G} .

3 Calibrating verbal autopsies

3.1 Naive calibration

Let $\mathbf{p} = (p_1, p_2, \dots, p_C)'$ denote the true CSMF in the country of interest where a large population set \mathcal{P} of only VA records and a small hospital set \mathcal{H} of paired VA and true-COD data is available. For a random VA record (list of symptoms) \mathbf{s} , we can write $p_i = P(G(\mathbf{s}) = i)$ where G denote the GS-COD for the individual. Also let $A(\mathbf{s}) = A(\mathbf{s} | \mathcal{P}, \mathcal{G})$ denote the predicted COD from the CCVA algorithm A trained on \mathcal{P} and some non local information \mathcal{G} . The naive estimate of CSMF from A is given by

$$\mathbf{q} = (q_1, q_2, \dots, q_C)' \text{ where } q_i = \int Pr(A(\mathbf{s} | \mathcal{P}, \mathcal{G}) = i) dP(\mathbf{s}).$$

When \mathcal{P} is an enumeration of a large number (N) of representative deaths in the country, we can approximate $q_i \approx \sum_{\{\mathbf{s} \in \mathcal{P}\}} I((A(\mathbf{s} | \mathcal{P}, \mathcal{G}) = i)) / N = v_i / N$, where v_i is the number of deaths in \mathcal{P} predicted by A to have occurred from cause i .

If we trust the algorithm A , one would consider \mathbf{q} to be a valid estimate of \mathbf{p} . More realistically, the reliance of A on non-local \mathcal{G} implies that its accuracy depends on how similar the algorithm A is in the new versus GS settings. Hence, more generally we can

think of q_i as the expected population prevalence of cause i that would be predicted by $A(\cdot \mid \mathcal{P}, \mathcal{G})$. The method-of-moments estimator of q_i is v_i/N .

In their most general form, G and A can be thought of as measurable functions from the high-dimensional symptom space to \mathcal{S}^C , the space of all C dimensional discrete distributions. Hence, we can write

$$A(\mathbf{s}) \sim \text{Categorical}(\mathbf{q}), G(\mathbf{s}) \sim \text{Categorical}(\mathbf{p}). \quad (1)$$

This only depicts the marginal distributions of $A(\mathbf{s})$ and $G(\mathbf{s})$. To infer about G from A , we model their joint distribution. We express $q_i = \sum_{j=1}^C m_{ij}p_j$ where $m_{ij} = p(A(\mathbf{s}) = j \mid G(\mathbf{s}) = i)$. In matrix notation, we have $\mathbf{q} = \mathbf{M}'\mathbf{p}$ where $\mathbf{M} = (m_{ij})$ is a transition matrix which we refer to as the *misclassification matrix*. First note that, if $\mathbf{M} = \mathbf{I}$, then $\mathbf{p} = \mathbf{q}$ and hence this subsumes the case where the VA-based algorithm is trusted and the resulting CSMFs \mathbf{q} are considered as reliable surrogates of the true CSMFs \mathbf{p} .

In settings relevant to our motivating COMSA application, we can opt to use the more general relationship $\mathbf{q} = \mathbf{M}'\mathbf{p}$ and estimate the misclassification rates m_{ij} 's from the hospital set \mathcal{H} . Let $n = \sum_{i=1}^C n_i$ denote the sample size of \mathcal{H} with n_i denoting the number of deaths from cause i . Also let $\mathbf{T} = (t_{ij})$ denote the error matrix for algorithm A , i.e. t_{ij} = number of deaths in \mathcal{H} from cause i that were attributed to cause j by A . It is clear that t_{ij}/n_i is a method-of-moments estimator of m_{ij} . In cases where there is substantial mismatch between the true and CCVA predicted COD in \mathcal{H} , we can use the error matrix \mathbf{T} to estimate \mathbf{M} which along with the earlier estimate of \mathbf{q} can lead to a substantially improved estimate of \mathbf{p} . Formally we can specify this via a hierarchical model as:

$$\begin{aligned} A(\mathbf{s}_r) &\stackrel{iid}{\sim} \text{Categorical}(\mathbf{M}'\mathbf{p}), r = 1, 2, \dots, N \\ \mathbf{T}_{i*} &\stackrel{ind}{\sim} \text{Multinomial}(n_i, \mathbf{M}_{i*}), i = 1, 2, \dots, C \end{aligned} \quad (2)$$

where for $r = 1, 2, \dots, N$, \mathbf{s}_r denote the list of symptoms obtained from the verbal autopsy of the r^{th} individual in \mathcal{P} , and for any matrix \mathbf{M} , \mathbf{M}_{i*} and \mathbf{M}_{*j} denote its i^{th} row and j^{th} column

respectively. The Categorical($\mathbf{M}'\mathbf{p}$) model for $A(\mathbf{s}_r)$ represents the relationship $\mathbf{q} = \mathbf{M}'\mathbf{p}$ and yields the method-of-moments estimators $\hat{\mathbf{q}} = (v_1, v_2, \dots, v_C)' / N$. The multinomial model for T_{i*} is consistent with the naive estimates t_{ij}/n_i of m_{ij} .

To estimate \mathbf{p} , one can adopt a modular approach where first $\hat{\mathbf{q}}$ and $\widehat{\mathbf{M}}$ are calculated separately and then obtain

$$\hat{\mathbf{p}} = \arg \min_{\mathbf{p}: \mathbf{1}'\mathbf{p}=1, p_i \geq 0} L(\hat{\mathbf{q}}, \widehat{\mathbf{M}}'\mathbf{p})$$

where L is some loss function like the squared-error or, more appropriately, the Kullback-Liebler divergence between the probability vectors. This approach fails to propagate the uncertainty in the estimation of \mathbf{M} in the final estimates of \mathbf{p} . Alternatively, an information-theoretically optimal solution would be to estimate the joint MLE of \mathbf{M} and \mathbf{p} from (2). In our implementation we chose the latter.

The advantage of the calibration approach is that it efficiently exploits the small local training data \mathcal{H} to reduce cross-country bias. Instead of trying to use \mathcal{H} to estimate the $P(\mathbf{s} \mid c)$ matrix, we now only use it to train a $p(A(\mathbf{s}) \mid c)$ misclassification matrix. One can view the predicted cause $A(\mathbf{s})$ as a one dimensional proxy symptom. Consequently, $p(A(\mathbf{s}) \mid c)$ involves only $C(C - 1)$ parameters as opposed to the $S(C - 1)$ parameters of the $p(s \mid c)$ matrix. S is typically 100 – 250 while we can choose C to be small focusing on the top 5 or 10 causes. Hence, the calibration approach achieves considerable dimension reduction by switching from the original symptom space to the predicted cause space.

In equation 2 above, \mathbf{q} can be estimated precisely because N is large. However, \mathbf{M} has $C \times (C - 1)$ parameters so that if there are many causes of interest, the estimates will have large variances owing to the small size of \mathcal{H} . Furthermore, data collection often spans a few years; in the early stages, \mathcal{H} may only have a very small sample size resulting in an extremely imprecise estimate of \mathbf{M} , even if we restrict to only the top few causes. Consequently, in the next section we propose a regularized approach that stabilizes the calibration.

3.2 Bayesian regularized calibration

If the hospital dataset \mathcal{H} was not available, i.e., no deaths in the new country had been assigned a true COD, we only have \mathcal{P} and some non-local GS information \mathcal{G} . Then it would be natural to train A using \mathcal{P} and \mathcal{G} and the resulting CSMF estimates \mathbf{q} would be the best guess for \mathbf{p} . This is equivalent to $\mathbf{p} = \mathbf{q}$ and $\mathbf{M} = \mathbf{I}$, i.e., assuming that the algorithm A is perfect. Extending this argument, when gold standard COD is available for a limited number of deaths \mathcal{H} , direct estimates of \mathbf{M} would be unstable and we should rely more on the CCVA algorithm. Hence, it is reasonable to shrink \mathbf{p} towards \mathbf{q} i.e., we shrink towards the default assumption that A is accurate. This is equivalent to shrinking the estimate of \mathbf{M} towards \mathbf{I} . The simplest way to achieve this is by using the regularized estimate $\widetilde{\mathbf{M}} = (1 - \lambda)\widehat{\mathbf{M}} + \lambda\mathbf{I}$ where $\widehat{\mathbf{M}} = (\widehat{m}_{ij}) = t_{ij}/n_i$ is the unshrunk method-of-moments estimate of m_{ij} as derived in the previous section. The regularized estimate $\widetilde{\mathbf{M}}$ (like $\widehat{\mathbf{M}}$ and \mathbf{M}) remains a transition matrix. The parameter λ quantifies the degree of shrinkage with $\lambda = 0$ yielding the unbiased method-of-moments estimate and $\lambda = 1$ leading to $\widehat{\mathbf{p}} = \widehat{\mathbf{q}}$. Hence, λ represents the bias variance trade-off for estimation of transition matrices and for small sample sizes some intermediate values of λ may lead to more precise estimates of \mathbf{M} and \mathbf{p} .

In practice, as data will come in batches over a period spanning few years, one needs to rerun the calibration procedure to update the CSMF. In the beginning, when \mathcal{H} is extremely small, it is expected that more regularization is required. Eventually, when \mathcal{H} becomes large, we could rely on the direct estimate $\widehat{\mathbf{M}}$. Hence, λ should be a function of the size n of \mathcal{H} , with $\lambda = 1$ for $n = 0$ and $\lambda \approx 0$ for large n . At intermediate stages, since the distribution of true COD in \mathcal{H} will be non-uniform, we will have a disparity in sample sizes n_i for estimating the different rows of \mathbf{M} . Consequently, it makes more sense to regularize each row of \mathbf{M} separately instead of using a single λ . A more flexible regularized estimate is given by $\widetilde{\mathbf{M}}_{i*} = (1 - \lambda_i)\widehat{\mathbf{M}}_{i*} + \lambda_i\mathbf{I}_{i*}$. The row specific weights λ_i should be chosen such that $\lambda_i = 1$ when $n_i = \sum_{j=1}^C t_{ij} = 0$, and $\lambda_i = 0$ when $\sum_{j=1}^C t_{ij} \rightarrow \infty$. One choice to accomplish

this is given by $\lambda_i = \gamma_i / (n_i + \gamma_i)$ for some fixed positive γ_i 's.

We now propose a hierarchical Bayesian formulation that accomplishes this regularized estimation of any transition matrix \mathbf{M} . We consider a Dirichlet prior $\mathbf{M}_{i*} \stackrel{ind}{\sim} \text{Dirichlet}(\gamma_i(\mathbf{I}_{i*} + \epsilon \mathbf{1}))$ for the rows of \mathbf{M} . It is easy to see that, using this prior, $\mathbf{M}_{i*} \mid \mathbf{T}_{i*}, \gamma_i \sim \text{Dirichlet}(\mathbf{T}_{i*} + \gamma_i(\mathbf{I}_{i*} + \epsilon \mathbf{1}))$. Hence, $E(\mathbf{M}_{i*} \mid \mathbf{T}_{i*}, \gamma_i) = (\mathbf{T}_{i*} + \gamma_i(\mathbf{I}_{i*} + \epsilon \mathbf{1})) / (n_i + \gamma_i(1 + C\epsilon)) \xrightarrow{\epsilon \rightarrow 0} (1 - \lambda_i)\mathbf{T}_{i*}/n_i + \lambda_i\mathbf{I}_{i*}$ where $\lambda_i = \gamma_i / (n_i + \gamma_i)$. Hence, in the limiting case for $\epsilon \rightarrow 0$, the Bayes estimator (posterior mean) for \mathbf{M} becomes equivalent with the desired shrinkage estimator proposed above. When $n = 0$, the Bayes estimate $E(\mathbf{M} \mid \mathbf{T}, \boldsymbol{\gamma} = (\gamma_1, \gamma_2, \dots, \gamma_C)') \rightarrow \mathbf{I}$, and when $n \rightarrow \infty$, $E(\mathbf{M} \mid \mathbf{T}, \boldsymbol{\gamma})$ becomes the method-of-moments estimator $\widehat{\mathbf{M}}$. Hence, the Dirichlet prior ensures that in data-scarce setting, \mathbf{M} is shrunk towards \mathbf{I} and consequently \mathbf{p} towards \mathbf{q} . In practice, we need to use a small $\epsilon > 0$ to ensure a proper posterior for \mathbf{M} when any off-diagonal entries of \mathbf{T} are zero, which is very likely due to the limited size of \mathcal{H} .

To complete the hierarchical formulation, we augment (2) with the priors:

$$\begin{aligned} \mathbf{M}_{i*} &\stackrel{ind}{\sim} \text{Dirichlet}(\gamma_i(\mathbf{I}_{i*} + \epsilon \mathbf{1})), i = 1, 2, \dots, C \\ \mathbf{p} &\sim \text{Dirichlet}(\delta \mathbf{1}) \\ \gamma_i &\stackrel{ind}{\sim} \text{Gamma}(\alpha, \beta), i = 1, 2, \dots, C \end{aligned} \tag{3}$$

Note that the calibration only uses the data from \mathcal{H} to estimate the conditional probabilities $P(A(\mathbf{s}) \mid c)$. We do not add the VA records for these deaths in the population set \mathcal{P} , i.e., we don't include them in the top row of (2). This is because for the small number of deaths in \mathcal{H} , the GS autopsies are conducted in one or two medical centers in a country and the marginal distribution of COD for deaths occurring in a hospital will possibly be very different from the population CSMFs in the new country. Due to economic constraints, the number of deaths for which a GS autopsy procedure will be conducted is often predetermined based on the project budget. Hence, the deaths for GS autopsy often will be chosen in a balanced way to represent most of the major causes in the country. Further variation in the cause of death distribution for \mathcal{H} is introduced due to uncertainty of obtaining consent for conducting

full autopsy. All of these virtually guarantee that even if \mathcal{H} consists of few hundred deaths with GS-COD, the marginal CSMF in \mathcal{H} is highly unlikely to represent the marginal CSMF in the population. Hence, we only use \mathcal{H} to estimate the conditional probabilities \mathbf{M} .

Our previous arguments, illustrating the shrinkage estimation of \mathbf{M} induced by the Dirichlet prior, are limited to the estimation of \mathbf{M} from \mathcal{H} as an independent piece and disregards the data and model for the population set \mathcal{P} , i.e. the first row of (2). In a hierarchical setup, however, the models for \mathcal{P} and \mathcal{H} contribute jointly to the estimation of \mathbf{M} and \mathbf{p} . We will now state a more general result that argues that even for the full hierarchical model specified through (2) and (3), when there is no local GS data or if the algorithm A demonstrates perfect accuracy on \mathcal{H} , then the marginal posterior estimates of \mathbf{p} after calibration coincides with the pre-calibration VA-based method-of-moments estimate $\hat{\mathbf{q}}$. Before stating the result, first note that the likelihood for $\mathbf{a} = (A(\mathbf{s}_1), A(\mathbf{s}_2), \dots, A(\mathbf{s}_N))'$ can be represented using the sufficient statistics $\mathbf{v} = (v_1, v_2, \dots, v_C)'$. We can write $p(\mathbf{a}) \propto \prod_{j=1}^C q_j^{v_j}$ and hence $\mathbf{p}, \mathbf{M}, \boldsymbol{\gamma} | \text{data} = \mathbf{p}, \mathbf{M}, \boldsymbol{\gamma} | \mathbf{v}, \mathbf{T}$.

Theorem 1. *If \mathbf{T} is a diagonal matrix, then $\lim_{\epsilon \rightarrow 0} \mathbf{p} | \mathbf{v}, \mathbf{T} \sim \text{Dirichlet}(\mathbf{v} + \delta \mathbf{1})$*

From Theorem 1, when \mathbf{T} is diagonal (including $\mathbf{T} = \mathbf{O}$), then the marginal posterior mean $E(\mathbf{p} | \mathbf{v}, \mathbf{T} = (v_i + \delta)/(N + C\delta))$. Choosing the hyper-parameter δ to be zero, this coincides with the method-of-moments estimate $\hat{\mathbf{q}} = \mathbf{v}/N$. In other words, Theorem 1 shows that if there is no hospital set available or if no misclassification is observed in \mathcal{H} , then for sufficiently small ϵ , the posterior mean of calibrated CSMF coincides with the uncalibrated estimates of CSMF obtained by directly using the VA algorithm. Note that Theorem 1 does not involve any assumption about the underlying data generation scheme or any asymptotic (large-sample) paradigm. In the best case scenario, when A is absolutely accurate for the new country, Theorem 1 shows that our calibration automatically recognizes this accuracy and does not modify the CSMF estimates from A . The result of Theorem 1 is confirmed in simulations in Section 5.

3.3 Gibbs sampler using augmented data

The joint posterior density can be expressed as

$$p(\mathbf{p}, \mathbf{M}, \boldsymbol{\gamma} \mid \mathbf{v}, \mathbf{T}) \propto p(\mathbf{v} \mid \mathbf{M}, \mathbf{p})p(\mathbf{T} \mid \mathbf{M})p(\mathbf{M} \mid \boldsymbol{\gamma})p(\mathbf{p})p(\boldsymbol{\gamma})$$

Let $\mathbf{p} \mid \cdot$ denote the full conditional distribution of \mathbf{p} . We use similar notation for other full conditionals. First note that since $p(\mathbf{v} \mid \mathbf{M}, \mathbf{p}) \propto \prod_j (\sum_i m_{ij} p_i)^{v_j}$, the full conditional densities $\mathbf{p} \mid \cdot$ and $\mathbf{M} \mid \cdot$ do not belong to any standard family of distributions, thereby prohibiting a direct Gibbs sampler. We here use a data augmentation scheme to efficiently implement a Gibbs sampler using conjugate distributions.

The term $(\sum_i m_{ij} p_i)^{v_j}$ can be expanded using the multinomial theorem, with each term corresponding to one of the partitions of v_j into C non-negative integers. Equivalently we can write

$$(\sum_i m_{ij} p_i)^{v_j} \propto E(\prod_i (m_{ij} p_i)^{b_{ij}}) \text{ where } \mathbf{b}_j = (b_{1j}, \dots, b_{Cj})' \sim \text{Multinomial}(v_j, \mathbf{1}/C).$$

Choosing $\mathbf{b}_1, \mathbf{b}_2, \dots, \mathbf{b}_C$ to be independent, we can express $\prod_j (\sum_i m_{ij} p_i)^{v_j} \propto E(\prod_j \prod_i (m_{ij} p_i)^{b_{ij}})$ where the proportionality constant only depends on the observed v_j 's. Using the augmented data matrix $\mathbf{B} = (\mathbf{b}_1, \mathbf{b}_2, \dots, \mathbf{b}_C) = (b_{ij})$, we can write the complete posterior as

$$p(\mathbf{p}, \mathbf{M}, \boldsymbol{\gamma}, \mathbf{B} \mid \mathbf{v}, \mathbf{T}) \propto \prod_j \prod_i (m_{ij} p_i)^{b_{ij}} \times \prod_i p_i^{\delta-1} \times \prod_i \gamma_i^{\alpha-1} \exp(-\beta \gamma_i) \times \prod_i \left(\frac{\Gamma(C \gamma_i \epsilon + \gamma_i)}{\Gamma(\gamma_i \epsilon)^{C-1} \Gamma(\gamma_i \epsilon + \gamma_i)} \prod_j (m_{ij})^{t_{ij} + \gamma_i \epsilon + \gamma_i \mathbf{1}(i=j) - 1} \right) \quad (4)$$

The full conditional distributions can now be updated as follows:

$$\begin{aligned} \mathbf{b}_j \mid \cdot &\sim \text{Multinomial}(v_j, \frac{1}{\sum_i M_{ij} p_i} (M_{1j} p_1, M_{2j} p_2, \dots, M_{Cj} p_C)') \\ \mathbf{M}_{i*} \mid \cdot &\sim \text{Dirichlet}(b_{i1} + \gamma_i \epsilon + t_{i1}, \dots, b_{ii} + \gamma_i \epsilon + t_{ii} + \gamma_i, \dots, b_{iC} + \gamma_i \epsilon + t_{iC}) \\ \mathbf{p} \mid \cdot &\sim \text{Dirichlet}(\sum_j b_{1j} + \delta, \dots, \sum_j b_{Cj} + \delta) \end{aligned}$$

Finally, we update γ_i 's using a metropolis random walk with log-normal proposal to sample from the full conditionals $p(\gamma_i \mid \cdot) \propto \frac{\Gamma(C \gamma_i \epsilon + \gamma_i)}{\Gamma(\gamma_i \epsilon)^{C-1} \Gamma(\gamma_i \epsilon + \gamma_i)} \gamma_i^{\alpha-1} \exp(-\beta \gamma_i) \prod_j m_{ij}^{\gamma_i \epsilon + \gamma_i \mathbf{1}(i=j)}$.

4 Ensemble calibration

The formulation in (2) and (3) clearly reveals that our calibration can use the output from any CCVA algorithm. Several CCVA algorithms have been implemented in publicly available software. In any particular analysis, the optimal CCVA is unknown. In this section, we extend the methodology from Section 3.2 to an ensemble calibration that uses the predictions from multiple CCVA algorithms.

Let there be K algorithms $A^{(1)}, A^{(2)}, \dots, A^{(K)}$ and let $\mathbf{a}^{(k)} = (a_1^{(k)}, a_2^{(k)}, \dots, a_N^{(k)})'$ be the predicted COD from the k^{th} algorithm for all the N deaths in \mathcal{P} . We expect variation among the predictions from the different methods and consequently among the CSMF vectors $\mathbf{q}^{(k)}$'s. Since the true population CSMF is unique, following Section 3.1 we can write $\mathbf{q}^{(k)} = (q_1^{(k)}, q_2^{(k)}, \dots, q_C^{(k)})' = \mathbf{M}^{(k)'} \mathbf{p}$ where $\mathbf{M}^{(k)} = (m_{ij}^{(k)})$ is the matrix of conditional probabilities (misclassification matrix) for the k^{th} method. The predicted COD for the r^{th} diseased individual by algorithm $A^{(k)}$, $a_r^{(k)}$, marginally follows a Categorical($\mathbf{q}^{(k)}$) distribution. However, since we have K such VA-based predictions for the same individual and the predictions are expected to be correlated, we need to look at the joint distribution. A realistic assumption is to assume that $a_r^{(1)}, a_r^{(2)}, \dots, a_r^{(K)}$ are independent conditional of $G(\mathbf{s}_r)$, i.e.

$$p(a_r^{(1)} = j_1, a_r^{(2)} = j_2, \dots, a_r^{(K)} = j_K \mid G(\mathbf{s}_r) = i) = \prod_{k=1}^K m_{ij_k}^{(k)}.$$

Once again drawing the analogy that the prediction vector $(a_r^{(1)}, a_r^{(2)}, \dots, a_r^{(K)})'$ is a smaller-dimensional list of proxy symptoms for the r^{th} individual, this assumption is akin to the naive Bayes assumption used to jointly model the probability of symptoms given the true COD in InsilicoVA and InterVA. This implies that the marginal independence of the $a_r^{(k)}$'s will not generally hold. Instead we will have

$$p(a_r^{(1)} = j_1, a_r^{(2)} = j_2, \dots, a_r^{(K)} = j_K) = \sum_{i=1}^C \left(\prod_{k=1}^K m_{ij_k}^{(k)} \right) p_i = q_{\mathbf{j}} \quad (5)$$

where $\mathbf{j} = (j_1, j_2, \dots, j_K)$ denotes a $C \times 1$ vector index.

For the limited number of deaths in the calibration set for which the true gold standard cause of death is available, the error matrices $\mathbf{T}^{(k)} = (t_{ij}^{(k)})$ are also known where $(t_{ij}^{(k)})$ is the number of deaths from cause i identified to be from cause j by the k^{th} algorithm. Using the $\mathbf{T}^{(k)}$'s the respective misclassification matrices $\mathbf{M}^{(k)}$'s can be estimated in the same way \mathbf{M} was estimated from \mathbf{T} in Section 3.1. Hence, the conditional independence assumption ensures that there is adequate data to estimate the enhanced number of parameters for this ensemble method. Subsequently, like the individual calibration model, we can regularize each $\mathbf{M}^{(k)}$ using Dirichlet priors.

Let \mathbf{q}^* denote a $C^K \times 1$ vector formed by stacking up all the q_{j_1, j_2, \dots, j_K} 's defined in (5). The full specifications for the ensemble calibration model that incorporates the predictions from all the algorithms is given by:

$$\begin{aligned} \mathbf{a}_r &= (a_r^{(1)}, a_r^{(2)}, \dots, a_r^{(K)}) \stackrel{ind}{\sim} \text{Categorical}(\mathbf{q}^*), r = 1, 2, \dots, N \\ \mathbf{T}_{i*}^{(k)} &\stackrel{ind}{\sim} \text{Multinomial}(n_i, \mathbf{M}_{i*}^{(k)}), i = 1, 2, \dots, C; k = 1, 2, \dots, K \\ \mathbf{M}_{i*}^{(k)} &\stackrel{ind}{\sim} \text{Dirichlet}(\gamma_i^{(k)}(\mathbf{I}_{i*} + \epsilon \mathbf{1})), i = 1, 2, \dots, C; k = 1, 2, \dots, K \\ \mathbf{p} &\sim \text{Dirichlet}(\delta \mathbf{1}) \\ \gamma_i^{(k)} &\stackrel{ind}{\sim} \text{Gamma}(\alpha, \beta), i = 1, 2, \dots, C; k = 1, 2, \dots, K \end{aligned} \quad (6)$$

The ensemble calibration ensures that predictions from all the used VA algorithms are incorporated in the final decision-making. The Gibbs sampler for (6) is provided in Section C of the Supplement. To understand how the different methods are given importance based on their accuracy on the hospital set \mathcal{H} , we present the following result:

Theorem 2. *If $\mathbf{T}^{(1)}$ is diagonal, and all entries of $\mathbf{T}^{(k)}$ are ≥ 1 for all $k > 1$, then $\mathbf{p} \mid \mathbf{v}, \mathbf{T}^{(1)}, \mathbf{T}^{(2)}, \dots, \mathbf{T}^{(K)} \sim \text{Dirichlet}(\mathbf{v}^{(1)} + \delta)$ where $\mathbf{v}^{(1)} = (v_1^{(1)}, v_2^{(1)}, \dots, v_C^{(1)})$, $v_i^{(k)}$ denoting the number of deaths assigned to cause i by algorithm k .*

Theorem 2 reveals that if one of the K algorithms produce perfect prediction on \mathcal{H} , then CSMF estimate from the ensemble calibration coincides with that of the individual calibration using that specific CCVA algorithm. The perfect agreement assumed in Theorem 2 will

not occur in practice. However, simulation and data analyses will confirm that the ensemble calibration tends to agree with the calibration from the more accurate CCVA algorithm. This offers a more efficient way to weight the multiple algorithms, yielding a unified CSMF estimate that is more robust to inclusion of an inaccurate CCVA algorithm in the decision making. In comparison, a simple average of CSMF from individual calibration models for each of the K algorithms would be more adversely affected by inaccurate algorithms.

4.1 Independent ensemble model

The joint ensemble model in Section 4 involves estimating the C^K multinomial vector \mathbf{q}^* whose entries are defined in (5). Even though there is a relatively large database of a few thousand VA records from the community-wide survey \mathcal{P} to estimate \mathbf{q}^* , this can only be implemented in practice if C is typically around 3 – 5 and K will be 2 or 3. There are many CCVA algorithms out there, and researchers often want to use all of them in an analysis. We also may be interested in more than 3 – 5 top causes. In such cases, there are too few instances for most combination of predicted causes for the K algorithms and most estimates of q_j 's will be zero. Also, the richly parametrized joint ensemble model imposes heavy computation demands with the Gibbs sampler (see Section C) introducing an additional C^K independent multinomial variables of dimension C thereby mandating long MCMC runs to achieve satisfactory convergence.

From equation (5), we note that

$$p(a_r^{(k)} = j_k) = \sum_{j_s: s \neq k} \sum_{i=1}^C \left(\prod_{k=1}^K m_{ij_k}^{(k)} \right) p_i = \sum_{i=1}^C m_{ij_k}^{(k)} p_i \quad (7)$$

by exchanging the summations. Hence, the marginal distribution of $a_r^{(k)}$ is Categorical($\mathbf{q}^{(k)}$) where $\mathbf{q}^{(k)} = (\mathbf{M}^{(k)})' \mathbf{p}$. This shows how the formulation of the ensemble model leads to the individual calibration model in Section 3.2 if we used only the predictions from the k^{th}

CCVA algorithm. It also allows us to model the $a_r^{(k)}$'s independently for each k as follows:

$$\mathbf{a}_r = (a_r^{(1)}, a_r^{(2)}, \dots, a_r^{(K)}) \stackrel{iid}{\sim} \prod_{k=1}^K \text{Categorical}(\mathbf{q}^{(k)}), r = 1, 2, \dots, N \quad (8)$$

Keeping the other specification same as in (6), we now have an independent ensemble model that only uses the marginal distributions of the $a_r^{(k)}$'s ignoring their joint dependence. While the total number of parameters for the joint and independent ensemble models remain the same, eliminating the joint model for each combination of predicted causes from the K algorithms disentangles the estimation of the $\mathbf{M}^{(k)}$ matrices. Additionally, the Gibbs sampler for the independent ensemble model is much simpler and closely resembles the individual calibration in Section 3.3. We only need to introduce K $C \times C$ matrices $\mathbf{B}^{(k)} = (\mathbf{b}_1^{(k)}, \mathbf{b}_2^{(k)}, \dots, \mathbf{b}_C^{(k)})$, one corresponding to each CCVA algorithm, akin to the matrix \mathbf{B} introduced in Section 3.3. If $\mathbf{v}^{(k)} = (v_1^{(k)}, v_2^{(k)}, \dots, v_C^{(k)})'$ denote the counts of predicted causes by algorithm k for the community-wide VA data, the Gibbs sampler steps for the independent ensemble model are:

$$\begin{aligned} \mathbf{b}_j^{(k)} \mid \cdot &\sim \text{Multinomial}(v_j^{(k)}, \frac{1}{\sum_i M_{ij}^{(k)} p_i} (M_{1j}^{(k)} p_1, M_{2j}^{(k)} p_2, \dots, M_{Cj}^{(k)} p_C)') \\ \mathbf{M}_{i*}^{(k)} \mid \cdot &\sim \text{Dirichlet}(b_{i1}^{(k)} + \gamma_i^{(k)} \epsilon + t_{i1}^{(k)}, \dots, b_{ii}^{(k)} + \gamma_i^{(k)} \epsilon + t_{ii}^{(k)} + \gamma_i^{(k)}, \dots, b_{iC}^{(k)} + \gamma_i^{(k)} \epsilon + t_{iC}^{(k)}) \\ \mathbf{p} \mid \cdot &\sim \text{Dirichlet}(\sum_k \sum_j b_{1j}^{(k)} + \delta, \dots, \sum_k \sum_j b_{Cj}^{(k)} + \delta) \end{aligned}$$

Observe that the sampler for the independent model uses CK additional parameters as opposed to C^K parameters introduced in the joint sampler. This ensures that the MCMC dimensionality does not exponentially increase if more CCVA algorithms are included in the ensemble model. The theoretical result in Theorem 2 no longer remains true for the independent model. However, our simulation results show that in practice it continues to put higher weights on the more accurate CCVA algorithm and consistently performs similar to or better than the joint model.

5 Simulation studies

The Population Health Metrics Research Consortium (PHMRC) study, conducted in 4 countries across six sites, is a benchmark database of paired VA records and GS-COD of children, neonates and adults. PHMRC data is frequently used to assess performance of CCVA algorithms. We conduct a set of simulation studies using the PHMRC data to generate a wide range of plausible scenarios where the performance of CCVA algorithms with and without calibration needs to be assessed. First, we randomly split the PHMRC child data (2064 samples) into three parts: gold standard, hospital and population sets, using a 2:1:2 ratio. This ensures that \mathcal{G} , \mathcal{H} and \mathcal{P} has roughly 800, 400 and 800 samples respectively. As accurate estimation of most prevalent causes are usually the priority, we restrict our attention to four causes: the top three most prevalent causes in the data from the country of interest ($\mathcal{H} \cup \mathcal{P}$) – Pneumonia, Diarrhea/Dysentery, Sepsis, and an *Other* cause grouping together all the remaining causes.

We wanted to simulate scenarios where both a) the cause-symptom dynamics are different in the new country of interest ($\mathcal{H} \cup \mathcal{P}$) and in the countries where gold standard data (\mathcal{G}) was collected from, and b) the marginal CSMF in \mathcal{P} is different from that in \mathcal{G} . Many CCVA methods, even when trained on a non-local \mathcal{G} , are robust to the latter source of difference, as demonstrated in the simulation studies in [McCormick et al. \(2016\)](#). However, if the cause-given-symptoms relationship are different in the new country, there is no way to learn that from \mathcal{G} on which the CCVA algorithm is trained.

Given a misclassification matrix $\mathbf{M} = (m_{ij})$ we want $P(A(\mathbf{s}) = j \mid G(\mathbf{s}) = i) = m_{ij}$ for any VA record $\mathbf{s} \in \mathcal{H} \cup \mathcal{P}$, where $G(\mathbf{s})$ and $A(\mathbf{s})$ respectively denote the GS-COD and predicted COD from algorithm A . We will achieve this by generating artificial GS-COD on $\mathcal{H} \cup \mathcal{P}$ such that a CCVA algorithm A trained on \mathcal{G} shows misclassification quantified by \mathbf{M} on $\mathcal{H} \cup \mathcal{P}$. Additionally, for any given probability vector $\mathbf{p}_{\mathcal{P}}$, which is different from the marginal CSMF in \mathcal{G} , we also want to ensure that the marginal CSMF in \mathcal{P} is $\mathbf{p}_{\mathcal{P}}$.

Note that if the true population CSMF needs to be $\mathbf{p}_{\mathcal{P}}$, then $\mathbf{q}_{\mathcal{P}}$, the population CSMF as predicted by A is given by $\mathbf{q}_{\mathcal{P}} = \mathbf{M}'\mathbf{p}_{\mathcal{P}}$. Hence, we first use A trained on \mathcal{G} to predict the COD for each record \mathbf{s} in the initial \mathcal{P} . We then resample \mathbf{s} from the initial \mathcal{P} to create a final \mathcal{P} such that the predicted COD of $A(\mathbf{s})$ has the marginal distribution $\mathbf{q}_{\mathcal{P}}$. Next, from Bayes theorem,

$$p(G(\mathbf{s}) = i \mid A(\mathbf{s}) = j) = \frac{P(A(\mathbf{s}) = j \mid G(\mathbf{s}) = i)P(G(\mathbf{s}) = i)}{\sum_i P(A(\mathbf{s}) = j \mid G(\mathbf{s}) = i)P(G(\mathbf{s}) = i)} = \frac{M_{ij}p_{\mathcal{P},i}}{\sum_i M_{ij}p_{\mathcal{P},i}} = \alpha_{ij}.$$

For \mathbf{s} in \mathcal{P} such that $A(\mathbf{s}) = j$, we generate a GS-COD from $\text{Categorical}((\alpha_{1j}, \alpha_{2j}, \dots, \alpha_{Cj})')$. This data generation process ensures that for any \mathbf{s} in \mathcal{P} both $G(\mathbf{s}) \sim \text{Categorical}(\mathbf{p}_{\mathcal{P}})$ and $A(\mathbf{s}) \mid G(\mathbf{s}) = i \sim \text{Categorical}(\mathbf{M}_{i*})$ are approximately true. We repeat the same procedure in \mathcal{H} , using the same \mathbf{M} but a different CSMF $\mathbf{p}_{\mathcal{H}}$. This reflects the reality where the symptom-given-cause dynamics are same for all deaths $\mathcal{H} \cup \mathcal{P}$ in the new country, but the hospital CSMF $\mathbf{p}_{\mathcal{H}}$ is unlikely to match the population CSMF $\mathbf{p}_{\mathcal{P}}$. For resampling to create the final \mathcal{H} , we also vary n — the size of \mathcal{H} as 50, 100, 200 and 400, to represent varying amount of local GS-data that will be available at different stages of a project.

We consider two choices of A : Tariff and Insilico. For \mathbf{M} , we use three choices – a diagonal matrix $\mathbf{M}_1 = \mathbf{I}$ – representing the case where the algorithm A is perfect for predicting COD in the new country, a matrix \mathbf{M}_2 with two large off-diagonal entries and all other off-diagonal ones being zero – representing the scenario where there are one or two systematic sources of bias in the COD predictions from A , and \mathbf{M}_3 which represents the scenario where there are many small misclassifications. Full specifications of the matrices are given in Section D in the Supplement. To ensure that the marginal CSMF in \mathcal{P} and \mathcal{H} are different, which is what we expect in reality, we generate pair of CSMFs $(\mathbf{p}_{\mathcal{H}}, \mathbf{p}_{\mathcal{P}})'$ from $\text{Dirichlet}(\mathbf{1})$ distribution. We consider three scenarios: *low*: $\text{CSMFA}(\mathbf{p}_{\mathcal{H}}, \mathbf{p}_{\mathcal{P}}) < 0.4$, *medium*: $0.4 < \text{CSMFA}(\mathbf{p}_{\mathcal{H}}, \mathbf{p}_{\mathcal{P}}) < 0.6$, and *high*: $\text{CSMFA}(\mathbf{p}_{\mathcal{H}}, \mathbf{p}_{\mathcal{P}}) > 0.6$. Here CSMFA denotes the CSMF accuracy which is a metric quantifying the difference in CSMF (Murray, Lozano, Flaxman, Vahdatpour & Lopez 2011). For each scenario, we generated 100 pairs, i.e. 300 pairs in total.

For each generated dataset, we fit the following models to predict the population CSMF $\mathbf{p}_{\mathcal{P}}$:

Table 2: List of models used to estimate population CSMF

Model name	Description
Tariff $_{\mathcal{G}}$	Tariff trained on the non-local gold standard data \mathcal{G}
Tariff $_C$	Calibrated VA using the output from Tariff $_{\mathcal{G}}$
Insilico $_{\mathcal{G}}$	InsilicoVA trained on the non-local gold standard data \mathcal{G}
Insilico $_C$	Calibrated VA using the output from Insilico $_{\mathcal{G}}$
Ensemble $_I$	Independent ensemble calibrated VA using outputs from Tariff $_{\mathcal{G}}$ and Insilico $_{\mathcal{G}}$

We present a brief summary of the results here. A much more detailed analysis is provided in Section D of the Supplement. For an estimate $\hat{\mathbf{p}}_{\mathcal{P}}(x)$ generate by a model x , we assess the performance of x using $\text{CSMFA}(x) = \text{CSMFA}(\hat{\mathbf{p}}_{\mathcal{P}}(x), \mathbf{p}_{\mathcal{P}}) = 1 - \frac{\|\hat{\mathbf{p}}_{\mathcal{P}}(x) - \mathbf{p}_{\mathcal{P}}\|_1}{2 \min \mathbf{p}_{\mathcal{P}}}$ (Murray, Lozano, Flaxman, Vahdatpour & Lopez 2011). Figure 1 presents the CSMFA for all the five models for the case when the data was generated using Tariff via the above design. The four rows correspond to four sizes of \mathcal{H} in increasing order, the three columns are for the three choices of \mathbf{M} described above, and in each figure the x -axis from left to right marks the *low*, *medium* and *high* settings for the CSMFA between the hospital set and the population set.

We first assess the performance of a VA algorithm, trained on \mathcal{G} , with our calibration approach using the output from that VA algorithm. This is the most relevant situation as VA data in a new country is customarily analyzed using a CCVA algorithm trained on non-local GS data. So, we intend to see if calibrating the CSMF using limited local GS data \mathcal{H} can improve estimates of CSMF. For Figure 1, this is the comparison between Tariff $_{\mathcal{G}}$ and Tariff $_C$. We see that, first for \mathbf{M}_1 , there is no difference in CSMFA between the two methods. This corroborates the theoretical result in Theorem 1 as \mathbf{M}_1 depicts the scenario where A is perfect. For \mathbf{M}_3 , which depicts the situation that the CCVA algorithm is reasonably accurate, we see that when both the size of \mathcal{H} is small and when the CSMFA between \mathcal{H}

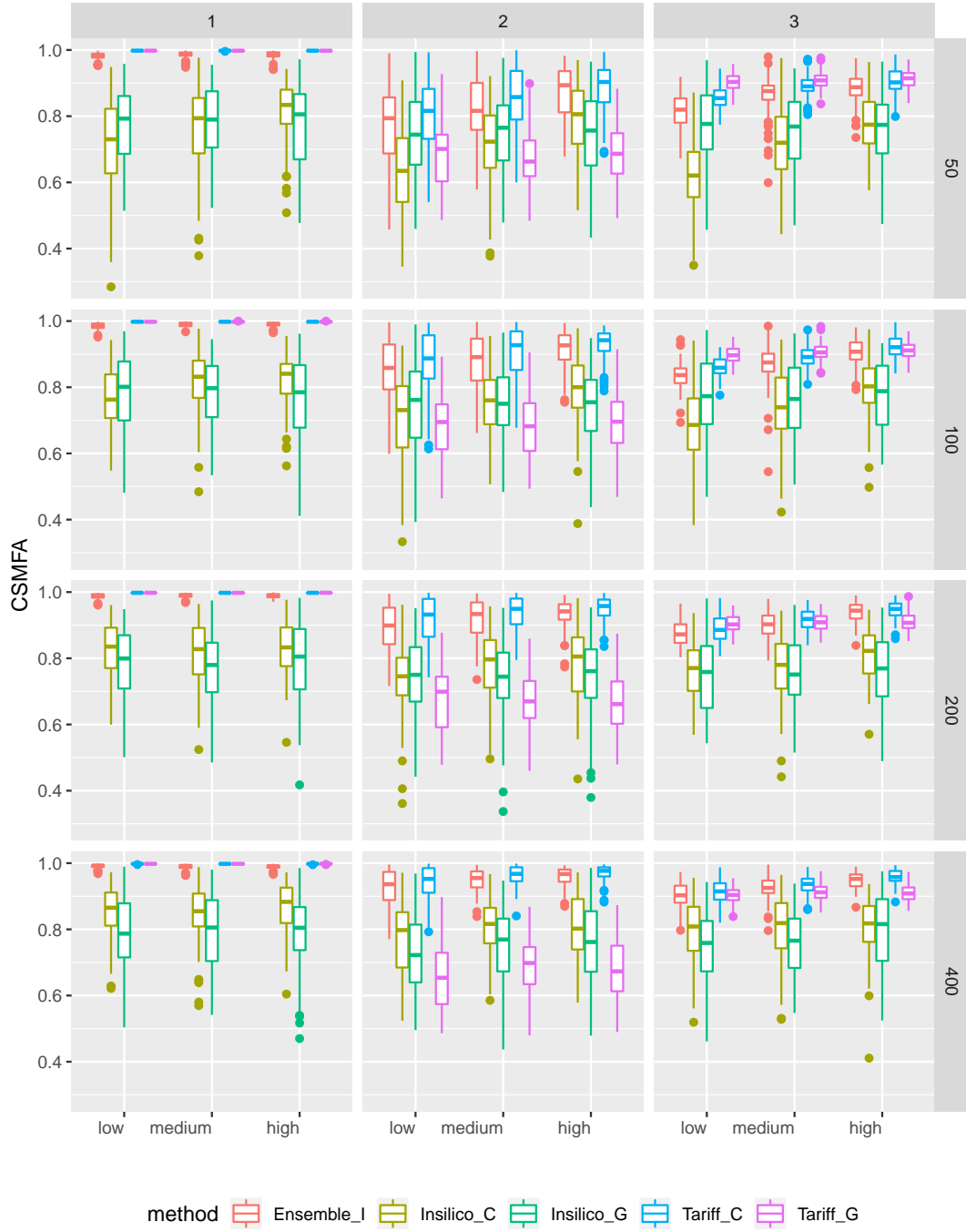


Figure 1: CSMF of ensemble and individual calibrations when data is generated using Tariff

and \mathcal{P} is low, i.e., there exists substantial disparity between the cause distribution in the hospital set and the population set, the calibrated CSMF from Tariff_C performs slightly worse than Tariff_G . When either increases, the performance of calibrated VA improves and Tariff_C performs better than Tariff_G with the improvements being substantial when n is large and CSMFA between \mathcal{H} and \mathcal{P} is high. Finally, for \mathbf{M}_2 , which depicts large bias for A , we see that the calibrated CSMF performs substantially better than its uncalibrated analogue across all scenarios. Since it is impossible to gauge apriori the accuracy of the uncalibrated CCVA, the results, across all three choices of \mathbf{M} , provide strong support for the use of the calibrated VA for reducing large biases.

Next we turn our attention to Insilico_G and Insilico_C . Since, the data was generated using Tariff , both performs much worse than their Tariff analogues. We see the reverse trends in Figure 9 of the supplement where the data was generated using InsilicoVA . This shows how in applications some CCVA algorithms can perform poorly and even after calibration may still yield subpar performance compared to some other CCVA algorithms. This is where the value of the ensemble model is evident, as we see that the CSMFA for Ensemble_I , which uses the output from both Tariff and InsilicoVA , is consistently closer to that of Tariff_C . In fact, for \mathbf{M}_1 , Ensemble_I produces CSMFA identical to Tariff_C which is what Theorem 2 suggests. Similarly, for data generated using Insilico , Figure 9 demonstrates how the performance of Ensemble_I aligns with that of Insilico_C which is the true model in that scenario. Since in practice we can never know which CCVA algorithm will be more accurate, the robustness offered by the ensemble sampler makes it a safer choice.

In Section D of the Supplement we present more thorough insights into the simulation study. In Section D.1 we assess the impact of the disparity in the CSMF between the non-local and the local data. In Section D.2 we compare the biases in the estimates of individual cause prevalence. Section D.3 delves into the role of the sample size and quality of the hospital set. Section D.4 demonstrates the value of the Bayesian shrinkage by comparing

with the frequentist calibration outlined in Section 3.1. In Section D.5 we compare the joint and independent ensemble calibration models and demonstrate how they favorably weight the more accurate CCVA algorithm. Finally, in Section D.6, we compare the performance of the models for predicting individual COD using the algorithm outlined in Section B.

6 Predicting CSMF in India and Tanzania

We evaluate the performance of calibrated and uncalibrated CCVA when predicting the CSMF for under 5 children in India and Tanzania using the PHMRC data. We could take advantage of the fact that PHMRC was conducted in multiple countries and our strategy was to sample records from a given country into the hospital and population sets $(\mathcal{H}, \mathcal{P})$, while treating all records from outside of the country as the non local gold standard set (\mathcal{G}) . We used the PHMRC child data to specifically focus on cause distribution for children deaths. This is important as the aforementioned COMSA projects currently only aim to conduct minimally invasive autopsies for children deaths under the age of five. We used both India and Tanzania, as they were the only countries with substantial enough sample sizes ($N_{India} = 948$, $N_{Tanzania} = 728$).

For a given country (either India or Tanzania), we first split the PHMRC child data into subjects from within the country $(\mathcal{H} \cup \mathcal{P})$ and from outside of the country (\mathcal{G}) . We then randomly selected $n(\in \{50, 100, 200, 400\})$ subjects from within the country of interest to be in \mathcal{H} , while the remaining subjects from within the country were put in \mathcal{P} . We trained models $Insilico_G$ and $Tariff_G$ using the non local data, which were then used to predict the top COD for all subjects in \mathcal{H} and \mathcal{P} . All predicted causes of death that are outside of the top K ($K \in \{3, 7\}$) COD within the country were changed to “Other”. These predictions were then used to estimate the calibrated CSMF for $Tariff_C$, $Insilico_C$, and $Ensemble_I$. Since the GS-COD is available in PHMRC, we calculated the true $\mathbf{p}_{\mathcal{P}}$ for a country as the empirical proportions of deaths from each cause, based on all the records within the country. This $\mathbf{p}_{\mathcal{P}}$

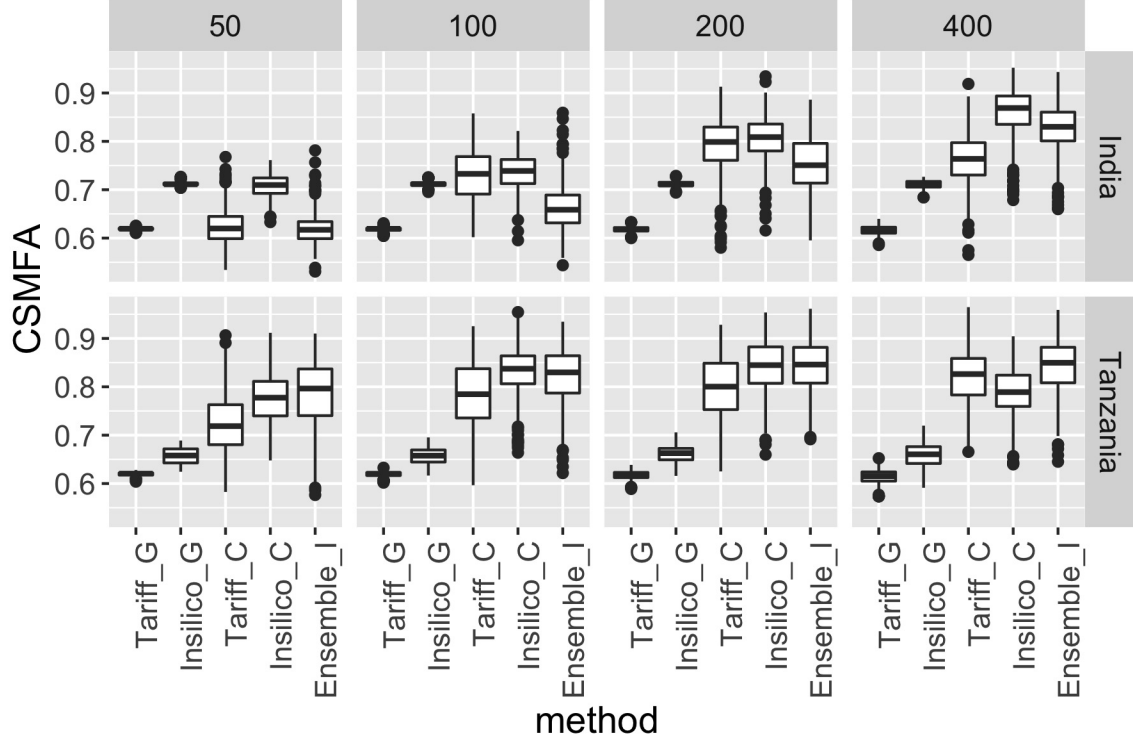


Figure 2: CSMFA using true GS-COD labels for the top 7 COD + others

was used to calculate the CSMFA of each of the models. This whole process was repeated 500 times for each combination of country, value of K , and value of n . This made sure that the results presented are average over 500 different random splits of \mathcal{H} and \mathcal{P} for each country, and are not for an arbitrary split.

Results from our analysis for $K = 7$ are shown in Figure 2 (figure for $K = 3$ shown in Supplemental Figure 13). The top and bottom rows represent the results for India and Tanzania respectively. The four columns correspond to four different choices of the size of the hospital set n . There are several striking observations. First, regardless of n , choice of algorithm A , and country, the calibrated estimates of prevalence significantly outperformed the analogous uncalibrated CSMFs, i.e., Tariff_C performed better than Tariff_G , and Insilico_C performed better than Insilico_G . Second, the magnitude of improvement for the calibrated

approach depends on the country and the size of the hospital set. Within India, the CSMFA of Tariff_C and Insilico_C is similar to those from Tariff_G and Insilico_G for $n = 50$, but increase dramatically as n increases and for $n = 200$ or 400 the CSMFA for Tariff_C and Insilico_C are almost 0.2 higher than the CSMFA for Tariff_G and Insilico_G respectively. In Tanzania, even for $n = 50$, we see that the calibrated CSMFA are substantially higher, which further increases with increasing n . In general, Insilico_G does better than Tariff_G and, in turn, Insilico_C is more accurate than Tariff_C . Again, the improvement of Insilico over tariff is more prominent in India than in Tanzania. Finally, the performance of Ensemble_I relative to Tariff_C and Insilico_C varies with n and country. In India, it appears to perform slightly worse than the individual calibration algorithms for smaller sample sizes, but when $n = 400$, CSMF from Ensemble_I is closer to the CSMF from the best CCVA algorithm (in this case Insilico). For Tanzania, Ensemble_I performs similar to or slightly better than both the individual calibration algorithms for all choices of n .

One caveat of this analysis is that we have fixed CSMF for the training and the test data, as determined empirically. Another downside is that, since we need to split the limited test set into a hospital and population set, as n increases, the sample size N of \mathcal{P} decreases. In fact, for Tanzania, when $n = 400$, there are more subjects in \mathcal{H} than in \mathcal{P} . Thus the impact of increase in sample size for the hospital set, is confounded by the decrease in sample size for the population set which can make the estimation less precise. In Section E of the Supplement we conduct a sensitivity analysis by resampling the records to create test and training set which display varying degrees of concordance in the cause distribution and where the population set has a fixed sample size.

7 MAP estimation

So far, we have only discussed fully Bayesian implementations of the calibration model in (3). If full inferential output is superfluous and only posterior point-estimates of the parameters

are desired, we outline a MAP (Maximum a posteriori) estimation for obtaining posterior modes of the parameters using an EM-algorithm. The data augmentation scheme introduced for the Gibbs sampler in 3.3 is also seamlessly congruous with the EM algorithm.

In particular, we consider the vector \mathbf{v} and \mathbf{T} as the observed data and augment \mathbf{B} introduced in Section 3.3 as the missing data to form the complete data likelihood $l(\mathbf{B}, \mathbf{v}, \mathbf{T} \mid \mathbf{M}, \mathbf{p}, \gamma)$ which is proportional to (4). At the s^{th} iteration, let $\mathbf{M}^{[s]} = (m_{ij}^{[s]})$, $\mathbf{p}^{[s]} = (p_i^{[s]})$ denote the current values of the parameters. Then

$$E^{[s]}(b_{ij} \mid \mathbf{v}, \mathbf{T}) = \frac{v_j m_{ij}^{[s]} p_i^{[s]}}{\sum_i m_{ij}^{[s]} p_i^{[s]}} = \hat{b}_{ij}^{[s]},$$

where $E^{[s]}$ denotes the expectation taken using the parameter values from the s^{th} iteration. The EM algorithm then proceeds as follows:

$$\begin{aligned} \text{E-step: } E^{[s]}(\log l(\mathbf{B}, \mathbf{v}, \mathbf{T} \mid \mathbf{M}, \mathbf{p}, \gamma) \mid \mathbf{v}, \mathbf{T}) = \sum_i \left(\sum_j \left(\hat{b}_{ij}^{[s]} \log(m_{ij} p_i) + \right. \right. \\ \left. \left. (t_{ij} + \gamma_i \epsilon + \gamma_i I(i=j) - 1) \log(m_{ij}) \right) + (\delta - 1) \log p_i + h(\gamma_i) \right) \end{aligned} \quad (9)$$

where $h(\gamma) = \log \left(\frac{\Gamma(C\gamma + \epsilon)}{\Gamma(\gamma\epsilon)^{C-1} \Gamma(\gamma\epsilon + \gamma)} \right) + (\alpha - 1) \log \gamma - \beta\gamma$. Subsequently, the maximization step can be formulated as:

$$\begin{aligned} \text{M-step: } m_{ij}^{[s+1]} &= \frac{\hat{b}_{ij}^{[s]} + t_{ij} + \gamma_i \epsilon + \gamma_i I(i=j) - 1}{\sum_j (\hat{b}_{ij}^{[s]} + t_{ij}) + \gamma_i C \epsilon + \gamma_i - C} \\ p_i^{[s+1]} &= \frac{\sum_j \hat{b}_{ij}^{[s]} + \delta - 1}{\sum_i \sum_j \hat{b}_{ij}^{[s]} + C\delta - C} \\ \gamma_i^{[s+1]} &= \arg \min \sum_i \sum_j (\gamma I(i=j) - 1) \log(m_{ij}) + h(\gamma) \end{aligned} \quad (10)$$

The closed form expression of \mathbf{M} and \mathbf{p} in the M-step is a consequence of the data augmentation. This drastically accelerates the MAP estimation as we only need to conduct C univariate optimizations, one corresponding to each γ_i . If instead the data augmentation was not exploited and only the observed likelihood was used, we would need to search an $O(C^2)$ dimensional space to obtain the MAP estimates. We can implement similar MAP

estimation algorithms for the joint and independent ensemble calibration models detailed in Section 4. We omit the steps here.

8 Demographic covariates and spatial information

The calibration approach introduced till this point focussed on generating national estimates of the CSMF \mathbf{p} . An important extension would be to model \mathbf{p} as a function of certain covariates like geographic region, social economic status (SES), sex and age groups. This will enable estimating regional and age-sex stratified CSMF which are also of interest for understanding the prevalence trends as well as guiding policy and allocation of resources aimed at improving public health. In this section, we demonstrate how to generalize the calibration model to accommodate covariates which can help us obtain a more detailed picture of the COD distribution within a country. We illustrate only for the individual calibration model based on a single CCVA algorithm. We can extend this for the ensemble model in the exact same manner.

Let \mathbf{x}_r denote a vector of covariates for the r^{th} VA record in \mathcal{P} . We propose the following modifications to the calibration model for allowing covariate-specific CSMFs $\mathbf{p}_r = (p_{r1}, p_{r2}, \dots, p_{rC})'$:

$$\begin{aligned} A(\mathbf{s}_r) &\overset{ind}{\sim} \text{Categorical}(\mathbf{M}'\mathbf{p}_r), r = 1, 2, \dots, N \\ p_{ri} &= \frac{\exp(\mathbf{x}_r'\boldsymbol{\beta}_i)}{\sum_{i=1}^C \exp(\mathbf{x}_r'\boldsymbol{\beta}_i)}, i = 1, 2, \dots, C, \boldsymbol{\beta}_C = 0 \\ \boldsymbol{\beta}_i &\overset{ind}{\sim} N(\mathbf{m}_{0i}, \mathbf{W}_{0i}) \end{aligned} \tag{11}$$

All other components of the original model in (2) and (3) remain unchanged. The middle row of (11) specify a multi-logistic model for the CSMFs using the covariates. The top row simply uses the covariate specific GS CSMF to model the analogous CSMF as would be predicted by A . Finally, the bottom row specifies Normal priors for the regression coefficients. The switch from a Dirichlet prior for \mathbf{p} to the multi-logistic model implies we can no longer directly

leverage conjugacy in the Gibbs sampler. [Polson et al. \(2013\)](#) proposed a Polya-Gamma data augmentation scheme to allow conjugate sampling for generalized linear models. We now show how our own data augmentation scheme introduced in Section 3.3 harmonizes with the Polya-Gamma sampler to create a streamlined Gibbs sampler.

8.1 Gibbs sampler using Polya-Gamma scheme

We will assume there are G unique combinations of covariate values—for example, if there are four geographic regions and three age groups, $G = 12$. If we have a continuous covariate, then $G = N$, where N is the number of subjects sampled in \mathcal{P} . Then letting g , $g = 1, \dots, G$, represent a specific covariate combination \mathbf{x}_g , we can again represent the likelihood for $\mathbf{a} = (A(\mathbf{s}_1), A(\mathbf{s}_2), \dots, A(\mathbf{s}_N))'$ using the $G \times C$ sufficient statistics $\mathbf{V} = (v_{gj})$ where v_{gi} is the total number of subjects with covariate values g that were predicted to have died of cause i . Let $\boldsymbol{\beta} = (\boldsymbol{\beta}_1, \boldsymbol{\beta}_2, \dots, \boldsymbol{\beta}_C)$. We now have

$$p(\mathbf{V} \mid \mathbf{M}, \boldsymbol{\beta}) \propto \prod_{g=1}^G \prod_{j=1}^C \left(\sum_{i=1}^C m_{ij} p_{gi} \right)^{v_{gj}}$$

and the joint posterior density can now be expressed as

$$p(\boldsymbol{\beta}, \mathbf{M}, \boldsymbol{\gamma} \mid \mathbf{V}, \mathbf{T}) \propto p(\mathbf{V} \mid \mathbf{M}, \boldsymbol{\beta}) p(\mathbf{T} \mid \mathbf{M}) p(\mathbf{M} \mid \boldsymbol{\gamma}) p(\boldsymbol{\beta}) p(\boldsymbol{\gamma})$$

The terms that are different from Section 3.3 are $p(\mathbf{V} \mid \mathbf{M}, \boldsymbol{\beta})$ and $p(\boldsymbol{\beta})$. The sampling step for $\boldsymbol{\gamma}$ remains exactly the same as previously discussed and is omitted here. We will use a similar data augmentation strategy as in Section 3.3 and combine with a Polya-Gamma data augmentation to sample from this posterior distribution. We expand the term

$$\left(\sum_i m_{ij} p_{gi} \right)^{v_{gj}} \propto E \left(\prod_i (m_{ij} p_{gi})^{b_{gij}} \right) \text{ where } \mathbf{b}_{gj} = (b_{g1j}, \dots, b_{gCj})' \stackrel{\text{ind}}{\sim} \text{Multinomial}(v_{gj}, \mathbf{1}/C).$$

Let \mathbf{B} denote the $GC \times C$ matrix formed by stacking all the \mathbf{b}_{gj} 's row-wise. We can write

$$p(\boldsymbol{\beta}, \mathbf{B}, \mathbf{M}, \boldsymbol{\gamma} \mid \mathbf{V}, \mathbf{T}) \propto \prod_g \prod_i \prod_j (m_{ij} p_{gi})^{b_{gij}} \times p(\mathbf{T} \mid \mathbf{M}) p(\mathbf{M} \mid \boldsymbol{\gamma}) p(\boldsymbol{\beta}) p(\boldsymbol{\gamma})$$

The following updates ensue immediately:

$$\begin{aligned} \mathbf{b}_{gj} \mid \cdot &\sim \text{Multinomial}(v_{gj}, \frac{1}{\sum_i M_{ij} p_{gi}} (M_{1j} p_{g1}, M_{2j} p_{g2}, \dots, M_{Cj} p_{gC})') \\ \mathbf{M}_{i*} \mid \cdot &\sim \text{Dirichlet}(\sum_g b_{gi1} + \gamma_i \epsilon + t_{i1}, \dots, \sum_g b_{gii} + \gamma_i \epsilon + t_{ii} + \gamma_i, \dots, \sum_g b_{giC} + \gamma_i \epsilon + t_{iC}) \end{aligned}$$

For β_i 's we introduce the Polya-Gamma variables ω_{gi} 's and define $\mathbf{\Omega}_i = \text{diag}(\{\omega_{gi}\}_{g=1}^G)$, $n_g = \sum_j v_{gj}$, and $\boldsymbol{\kappa}_i = (\kappa_{1i}, \dots, \kappa_{Gi})'$ where $\kappa_{gi} = \sum_j b_{gij} - n_g/2$. We then have

$$\begin{aligned} \omega_{gi} \mid \cdot &\sim PG(n_g, \mathbf{x}_g^T \boldsymbol{\beta}_i - c_{gi}) \text{ where } c_{gi} = \log(\sum_{k \neq i} \exp(x_g^T \beta_k)) \\ \boldsymbol{\beta}_i \mid \cdot &\sim \mathcal{N}(\mathbf{m}_i, \mathbf{W}_i) \text{ where } \mathbf{W}_i^{-1} = \mathbf{X}' \mathbf{\Omega}_i \mathbf{X} + \mathbf{W}_{0i}^{-1}, \mathbf{m}_i = \mathbf{W}_i (\mathbf{X}' (\boldsymbol{\kappa}_i - \mathbf{\Omega}_i \mathbf{c}_i) + \mathbf{W}_{0i}^{-1} \mathbf{m}_{0i}) \end{aligned}$$

Here PG denotes the Polya-Gamma distribution and $\mathbf{c}_i = (c_{1i}, c_{2i}, \dots, c_{Gi})'$. This completes the steps of a Gibbs sampler where all the parameters except $\boldsymbol{\gamma}$ are updated via sampling from conjugate distributions. We can transform the posterior samples of $\boldsymbol{\beta}$ to obtain posterior samples of p_{gi} . Estimates of the marginal CSMF for the whole country can also be obtained by using the relationship $p_i = \int p_{gi} dP(g)$.

Note that in the model above, we have assumed that the transition matrix is independent of the covariates. We can also introduce covariates in modeling the conditional probabilities m_{ij} 's using a similar multi-logistic regression. This will be particularly useful if there is prior knowledge about covariate-dependent systematic biases in the predictions from a CCVA algorithm. We can then nicely incorporate this information into the model. The implementation will then involve Polya-Gamma samplers for each row of \mathbf{M} in a manner exactly similar to the sampler outlined above. Hence, we do not include this here.

9 Discussion

Automating the prediction of cause of death (COD) from symptoms data is a challenging problem due to the high-dimension of the symptom-space, and complex and possibly varying

cause-symptom relationships. In our setting where a population-wide verbal autopsy (VA) survey is being conducted (COMSA examples) but where there are few observations of the true COD, the CCVA has to rely on non-local training data and hence is expected to be biased. We have proposed a novel calibration approach where the non-local GS data is used to train the CCVA as is customary, but additionally, the local GS data is used to calibrate the CCVA. The fully Bayesian implementation is fast, owing to a novel data-augmented Gibbs sampler. The ensemble calibration ensures robust estimates via averaging over CCVA methods and reduces the risk of selecting a poor CCVA for a particular population. Our simulations demonstrate the value of local calibration, offering substantially improved accuracy. The PHMRC data analysis makes evident the value of collecting a limited number of GS-COD in the local population using full or minimally invasive autopsies and then using calibration to improve CSMF estimates. The results also show how calibration benefits from larger sample sizes of the local (hospital) set, and from true cause of death prevalences in the hospital being more representative of the population.

Although motivated by the VA data, our methods can be more generally viewed as a way to locally calibrate any discrete classifiers trained on some high-dimensional non-local data. Hence, our calibration approach can be applied for any classification problem which involves estimating population numbers or fractions for a category of things based on limited local labeled (GS) data (\mathcal{H}), abundant local unlabeled data (\mathcal{P}) and abundant non-local labeled data (\mathcal{G}). For example, in recent years complex machine learning (ML) algorithms have been developed for image classification, which are trained on massive datasets of images scraped from the internet. Our calibration model can be potentially used to locally calibrate any of these ML algorithms to predict in a setting with limited training data. Analogously, the ensemble calibration can jointly work with multiple such algorithms and reduce the risk of choosing a single ML algorithm which may perform poorly. Hence, we can view the proposed calibration framework as a model-based approach to what is frequently referred in

the ML literature as *transfer learning*.

The concept of shrinkage or regularization is at the core of our calibration approach. With increasing dimensions of modern datasets, regularized methods have become ubiquitous. A vast majority of the literature focuses on shrinking estimates (mostly regression coefficients and covariance or precision matrices) towards some known sub-model. We apply the same principle of regularization in a unique way for estimating the population CSMF. Instead of shrinking towards any underlying assumptions about the true population CSMF, we shrink towards the estimate from the uncalibrated CCVA, as in absence of sufficient local data, that is the best available estimate. So our shrinkage harmonizes nicely with the idea of calibration which is to fine tune a reasonably good algorithm to improve its performance. We show how this shrinkage for the population CSMF is equivalent to shrinking the misclassification matrix towards the identity matrix. Subsequently, we show how properly chosen Dirichlet priors can achieve this shrinkage for a misclassification or transition matrix. This regularized estimation of a transition matrix can also be applied in other contexts.

Returning to the VA data, one important direction forward would be to generalize this approach for more complex COD outcomes. Currently COD outcome is viewed as a discrete variable taking values on a set of causes like Pneumonia or Sepsis etc. In practice, death is a complex chronological series of several events starting from some root causes and ending at the immediate or proximal cause. In addition to understanding prevalence of causes in the population, another goal for many of the aforementioned programs is to identify medical events that occurred before death for which an intervention could have helped prevent or delay mortality. Extending the current setup for hierarchical or tree-structured COD outcome would be a useful step towards this aim. Many CCVA algorithms, in addition to predicting the most likely COD, also predict the (posterior) distribution of likely causes. Our current implementation only uses the most likely COD as an input. An extension enabling the use of the full predictive distribution as an input can improve the calibration method. In par-

ticular, this will benefit the individual COD predictions for which currently two individuals with the same predicted COD from CCVA have the same predicted COD distribution after calibration. Finally, the VA data, containing about 250 questions for thousands of individuals, naturally has several erroneous entries. Currently preprocessing VA records to eliminate absurd entries and records entails onerous manual labor. It is challenging to develop quality control models for VA data due to the high dimensionality of the symptoms. Akin to what we did here, one can consider dimension reduction via the predictions of CCVA algorithms to create an automated statistical quality control for VA records.

SUPPLEMENTARY MATERIAL

Appendix: Contains proofs of Theorems 1 and 2, calibration of individual COD predictions, the Gibbs sampler for the joint ensemble calibration model, detailed analysis of the simulated data, the sensitivity analysis for the PHMRC data for India and Tanzania, and additional figures.

R-package calibratedVA: R-package calibratedVA containing code to perform the local calibration using predictions from a verbal autopsy algorithm to predict population CSMF is available at <https://github.com/jfiksiel/CalibratedVA/>. The package also contains the code for the ensemble calibration model for using outputs from several VA algorithms. A vignette describing how to navigate the package and demonstrating the use of the methodology is provided in <https://github.com/jfiksiel/CalibratedVA/blob/master/vignettes/CalibratedVA.Rmd>

References

AbouZahr, C., De Savigny, D., Mikkelsen, L., Setel, P. W., Lozano, R., Nichols, E., Notzon, F. & Lopez, A. D. (2015), ‘Civil registration and vital statistics: progress in the data revolution for counting and accountability’, *The Lancet* **386**(10001), 1373–1385.

- Allotey, P. A., Reidpath, D. D., Evans, N. C., Devarajan, N., Rajagobal, K., Bachok, R., Komahan, K. & Team, S. (2015), ‘Let’s talk about death: data collection for verbal autopsies in a demographic and health surveillance site in malaysia’, *Global health action* **8**(1), 28219.
- Byass, P. (2016), ‘Minimally invasive autopsy: A new paradigm for understanding global health?’, *PLoS medicine* **13**(11), e1002173.
- Byass, P., Chandramohan, D., Clark, S. J., D’ambruso, L., Fottrell, E., Graham, W. J., Herbst, A. J., Hodgson, A., Hounton, S., Kahn, K. et al. (2012), ‘Strengthening standardised interpretation of verbal autopsy data: the new interval-4 tool’, *Global health action* **5**(1), 19281.
- CJL, M., AD, L., R, B. & et al. (2011), ‘Population health metrics research consortium gold standard verbal autopsy validation study: design, implementation, and development of analysis datasets’, *Population Health Metrics* pp. 9–27.
- Flaxman, A. D., Joseph, J. C., Murray, C. J., Riley, I. D. & Lopez, A. D. (2018), ‘Performance of insilicova for assigning causes of death to verbal autopsies: multisite validation study using clinical diagnostic gold standards’, *BMC medicine* **16**(1), 56.
- James, S. L., Flaxman, A. D. & Murray, C. J. (2011), ‘Performance of the tariff method: validation of a simple additive algorithm for analysis of verbal autopsies’, *Population Health Metrics* **9**(1), 31.
- Kalter, H. D., Roubanatou, A.-M., Koffi, A. & Black, R. E. (2015), ‘Direct estimates of national neonatal and child cause-specific mortality proportions in niger by expert algorithm and physician-coded analysis of verbal autopsy interviews’, *Journal of global health* **5**(1).
- King, G., Lu, Y. et al. (2008), ‘Verbal autopsy methods with multiple causes of death’, *Statistical Science* **23**(1), 78–91.

- Leitao, J., Desai, N., Aleksandrowicz, L., Byass, P., Miasnikof, P., Tollman, S., Alam, D., Lu, Y., Rath, S. K., Singh, A. et al. (2014), ‘Comparison of physician-certified verbal autopsy with computer-coded verbal autopsy for cause of death assignment in hospitalized patients in low-and middle-income countries: systematic review’, *BMC medicine* **12**(1), 22.
- McCormick, T. H., Li, Z. R., Calvert, C., Crampin, A. C., Kahn, K. & Clark, S. J. (2016), ‘Probabilistic cause-of-death assignment using verbal autopsies’, *Journal of the American Statistical Association* **111**(515), 1036–1049.
- Murray, C. J., Lopez, A. D., Black, R., Ahuja, R., Ali, S. M., Baqui, A., Dandona, L., Dantzer, E., Das, V. & Dhingra, Usha, e. a. (2011), ‘Population health metrics research consortium gold standard verbal autopsy validation study: design, implementation, and development of analysis datasets’, *Population health metrics* **9**(1), 27.
- Murray, C. J., Lozano, R., Flaxman, A. D., Vahdatpour, A. & Lopez, A. D. (2011), ‘Robust metrics for assessing the performance of different verbal autopsy cause assignment methods in validation studies’, *Population health metrics* **9**(1), 28.
- Nichols, E. K., Byass, P., Chandramohan, D., Clark, S. J., Flaxman, A. D., Jakob, R., Leitao, J., Maire, N., Rao, C., Riley, I. et al. (2018), ‘The who 2016 verbal autopsy instrument: An international standard suitable for automated analysis by interval, insilicova, and tariff 2.0’, *PLoS medicine* **15**(1), e1002486.
- Polson, N. G., Scott, J. G. & Windle, J. (2013), ‘Bayesian inference for logistic models using pólya–gamma latent variables’, *Journal of the American statistical Association* **108**(504), 1339–1349.
- Serina, P., Riley, I., Stewart, A., James, S. L., Flaxman, A. D., Lozano, R., Hernandez, B., Mooney, M. D., Luning, R., Black, R. et al. (2015), ‘Improving performance of the tariff method for assigning causes of death to verbal autopsies’, *BMC medicine* **13**(1), 291.

Soleman, N., Chandramohan, D. & Shibuya, K. (2006), ‘Verbal autopsy: current practices and challenges’, *Bulletin of the World Health Organization* **84**, 239–245.

A Proofs

Proof of Theorem 1. The marginal posterior $\mathbf{p} \mid \mathbf{v}, \mathbf{T}$ is given by $\int p(\mathbf{p}, \mathbf{M}, \boldsymbol{\gamma} \mid \mathbf{v}, \mathbf{T}) dP(\mathbf{M}) dP(\boldsymbol{\gamma})$. Conditional on $\boldsymbol{\gamma}$, looking only at terms that involve \mathbf{p} , \mathbf{M} , and $\boldsymbol{\gamma}$, we have

$$p(\mathbf{p}, \mathbf{M}, \mathbf{v}, \mathbf{T} \mid \boldsymbol{\gamma}) \propto \prod_j \left(\sum_i m_{ij} p_i \right)^{v_j} \times \prod_i p_i^{\delta-1} \times \prod_i \frac{\Gamma(\gamma_i(C\epsilon + 1))}{(\Gamma(\gamma_i\epsilon))^{C-1} \Gamma(\gamma_i(\epsilon + 1))} \prod_j (m_{ij})^{t_{ij} + \gamma_i(\epsilon + 1(i=j)) - 1}$$

We will now use the multinomial theorem to expand the first product $\prod_j (\sum_i m_{ij} p_i)^{v_j}$. Note that the j^{th} term expands into $\kappa_j = \binom{v_j + C - 1}{C - 1}$ terms, one corresponding to each partition of v_j . Let $\mathbf{B}^{(j)} = (b_{ki}^{(j)})$ denote the $\kappa_j \times C$ partition matrix formed by stacking up all $1 \times C$ rows that represent a non-negative integer partition of v_j . The k^{th} row of $\mathbf{B}^{(j)}$ gives the k^{th} partition and i^{th} element of that row corresponds to power index for the i^{th} term ($m_{ij} p_i$). We now have,

$$\begin{aligned} p(\mathbf{p}, \mathbf{M} \mid \mathbf{v}, \mathbf{T}, \boldsymbol{\gamma}) &\propto \left(\prod_j \sum_{k_j=1}^{\kappa_j} \prod_i \frac{(m_{ij} p_i)^{b_{k_j i}^{(j)}}}{b_{k_j i}^{(j)}!} \right) \times \prod_i p_i^{\delta-1} \times \\ &\quad \prod_i \frac{\Gamma(\gamma_i(C\epsilon + 1))}{(\Gamma(\gamma_i\epsilon))^{C-1} \Gamma(\gamma_i(\epsilon + 1))} \prod_j (m_{ij})^{t_{ij} + \gamma_i(\epsilon + 1(i=j)) - 1} \\ &\propto \sum_{k_1=1}^{n_1} \cdots \sum_{k_C=1}^{n_C} \left(\prod_i \frac{\Gamma(\gamma_i(C\epsilon + 1)) p_i^{\sum_j b_{k_j i}^{(j)} - 1}}{(\Gamma(\gamma_i\epsilon))^{C-1} \Gamma(\gamma_i(\epsilon + 1))} \prod_j \frac{(m_{ij})^{b_{k_j i}^{(j)} + t_{ij} + \gamma_i(\epsilon + 1(i=j)) - 1}}{b_{k_j i}^{(j)}!} \right) \end{aligned}$$

Note that for a given k_1, \dots, k_C and i , the product $\prod_{j=1}^C (m_{ij})^{b_{k_j i}^{(j)} + t_{ij} + \gamma_i(\epsilon + 1(i=j)) - 1}$ is the kernel of a *Dirichlet* $(b_{k_1 i}^{(1)} + t_{i1} + \gamma_i\epsilon, \dots, b_{k_i i}^{(i)} + t_{ii} + \gamma_i(\epsilon + 1), \dots, b_{k_C i}^{(C)} + t_{iC} + \gamma_i\epsilon)$ distribution. Hence, integrating \mathbf{M} out with respect to the order $\prod_{i=1}^C \prod_{j=1}^C dm_{ij}$, we are left with

$$p(\mathbf{p} \mid \mathbf{v}, \mathbf{T}, \boldsymbol{\gamma}) \propto \sum_{k_1=1}^{n_1} \cdots \sum_{k_C=1}^{n_C} w_{k_1, k_2, \dots, k_C}(\boldsymbol{\gamma}, \epsilon) \prod_i p_i^{\sum_j b_{k_j i}^{(j)} + \delta - 1}$$

where $w_{k_1, k_2, \dots, k_C}(\gamma, \epsilon) = \prod_i \frac{\Gamma(\gamma_i(C\epsilon+1)) \prod_{j=1}^C \Gamma(b_{k_j i}^{(j)} + t_{ij} + \gamma_i(\epsilon+1(i=j)))}{(\Gamma(\gamma_i\epsilon))^{C-1} \Gamma(\gamma_i(\epsilon+1)) \Gamma(\sum_j (b_{k_j i}^{(j)} + t_{ij}) + \gamma_i(C\epsilon+1)) \prod_j b_{k_j i}^{(j)}}$. Hence,

$$\mathbf{p} \mid \mathbf{v}, \mathbf{T} \sim \sum_{k_1=1}^{n_1} \cdots \sum_{k_C=1}^{n_C} \left(\int \frac{1}{W(\gamma, \epsilon)} w_{k_1, k_2, \dots, k_C}(\gamma, \epsilon) dF(\gamma) \right) \text{Dirichlet}(\sum_j b_{k_j 1}^{(j)} + \delta, \dots, \sum_j b_{k_j C}^{(j)} + \delta)$$

where $W(\gamma, \epsilon) = \sum_{k_1=1}^{n_1} \cdots \sum_{k_C=1}^{n_C} w_{k_1, k_2, \dots, k_C}(\gamma, \epsilon)$. Without loss of generality, let the first row of each $\mathbf{B}^{(j)}$ represent the partition of v_j which allocates v_j to the j^{th} component and 0 to all the other components. For any $(k_1, k_2, \dots, k_C)' \neq \mathbf{1}_C$, we have

$$\lim_{\epsilon \rightarrow 0} \frac{w_{k_1, k_2, \dots, k_C}(\gamma, \epsilon)}{w_{1, 1, \dots, 1}(\gamma, \epsilon)} = \prod_i \frac{\Gamma(\sum_j t_{ij} + v_i + \gamma_i) \Gamma(b_{k_i i}^{(i)} + t_{ii} + \gamma_i)}{\Gamma(\sum_j (b_{k_j i}^{(j)} + t_{ij}) + \gamma_i) \Gamma(v_i + t_{ii} + \gamma_i)} \left(\prod_{j \neq i} \lim_{\epsilon \rightarrow 0} \frac{\Gamma(b_{k_j i}^{(j)} + t_{ij} + \gamma_i \epsilon)}{\Gamma(t_{ij} + \gamma_i \epsilon)} \right)$$

If $b_{k_j i}^{(j)} = 0$, the ratio $\frac{\Gamma(b_{k_j i}^{(j)} + t_{ij} + \gamma_i \epsilon)}{\Gamma(t_{ij} + \gamma_i \epsilon)}$ is one. However, since $(k_1, k_2, \dots, k_C)' \neq \mathbf{1}_C$, we have atleast one pair $i \neq j$ such that $b_{k_j i}^{(j)} \geq 1$ and consequently

$$\frac{\Gamma(b_{k_j i}^{(j)} + t_{ij} + \gamma_i \epsilon)}{\Gamma(t_{ij} + \gamma_i \epsilon)} = \prod_{s=0}^{b_{k_j i}^{(j)} - 1} (s + t_{ij} + \gamma_i \epsilon) \xrightarrow{\epsilon \rightarrow 0} 0$$

since T is diagonal. Hence, $w_{1, 1, \dots, 1}$ dominates all the other weights in the limiting case. Since each of the scaled weights are less than one, using dominated convergence theorem,

$$\lim_{\epsilon \rightarrow 0} \int \frac{1}{W(\gamma, \epsilon)} w_{k_1, k_2, \dots, k_C}(\gamma, \epsilon) dF(\gamma) = 1((k_1, k_2, \dots, k_C)' = \mathbf{1})$$

and hence $\lim_{\epsilon \rightarrow 0} p(\mathbf{p} \mid \mathbf{v}, \mathbf{T}) \propto \prod_i p_i^{\sum_j b_{1i}^{(j)} + \delta - 1} = \prod_i p_i^{v_i + \delta - 1}$.

□

Proof of Theorem 2. We proof only for the case $K = 2$ as the same proof generalizes for arbitrary K . We simplify the notation for the proof. Let v_{st} denote the number of VA deaths assigned to cause s by algorithm 1, and cause t by algorithm 2. We write $\mathbf{M}^{(1)} = \mathbf{M}$, $\mathbf{M}^{(2)} = \mathbf{N}$, $\mathbf{T}^{(1)} = \mathbf{T}$ and $\mathbf{T}^{(2)} = \mathbf{U}$ to get rid of the superscripts. Also, let $\mathbf{B}_{(st)} = (b_{li}^{(st)})$ denote a $\kappa_{st} \times C$ matrix formed by stacking row-wise all possible partitions of v_{st} into C

non-negative integers. Here $\kappa_{st} = \binom{v_{st}+C-1}{C-1}$ denotes the total number of such partitions. Let $\mathbf{h} = (h_{11}, h_{12}, \dots, h_{CC})'$ denote a generic index vector such that each $h_{st} \in \{1, 2, \dots, \kappa_{st}\}$ indexes to a partition of v_{st} and \mathcal{H} denote the collection of all such \mathbf{h} 's. Then likelihood for $(\mathbf{a}_1, \mathbf{a}_2, \dots, \mathbf{a}_N)'$ is

$$\begin{aligned} \prod_{s=1}^C \prod_{t=1}^C \left(\sum_{l=1}^{\kappa_{st}} \prod_{i=1}^C \frac{(p_i m_{is} n_{it})^{b_{li}^{(st)}}}{b_{li}^{(st)}!} \right) &= \sum_{\mathbf{h} \in \mathcal{H}} \prod_{i=1}^C \prod_{s=1}^C \prod_{t=1}^C \frac{(p_i m_{is} n_{it})^{b_{h_{st}i}^{(st)}}}{b_{h_{st}i}^{(st)}!} \\ &= \sum_{\mathbf{h} \in \mathcal{H}} \frac{1}{c_{\mathbf{h}}} \prod_{i=1}^C p_i^{\sum_{s=1}^C \sum_{t=1}^C b_{h_{st}i}^{(st)}} \prod_{s=1}^C m_{is}^{\sum_{t=1}^C b_{h_{st}i}^{(st)}} \prod_{t=1}^C n_{it}^{\sum_{s=1}^C b_{h_{st}i}^{(st)}} \end{aligned}$$

where $c_{\mathbf{h}}$ is a constant term free of the parameters.

Incorporating the priors and marginalizing with respect to \mathbf{M} and \mathbf{N} we have

$$\begin{aligned} p(\mathbf{p} \mid \mathbf{v}^*, \mathbf{T}, \mathbf{U}, \boldsymbol{\gamma}^{(1)}, \boldsymbol{\gamma}^{(2)}) &\propto \sum_{\mathbf{h} \in \mathcal{H}} \frac{1}{c_{\mathbf{h}}} \prod_{i=1}^C \left(p_i^{\sum_{s=1}^C \sum_{t=1}^C b_{h_{st}i}^{(st)} + \delta - 1} \times \right. \\ &\quad \frac{\prod_{s=1}^C \Gamma(\sum_{t=1}^C b_{h_{st}i}^{(st)} + t_{is} + \gamma_i^{(1)}(\epsilon + I(i=s)))}{\Gamma(\sum_{s=1}^C (\sum_{t=1}^C b_{h_{st}i}^{(st)} + t_{is}) + \gamma_i^{(1)}(C\epsilon + 1))} \times \\ &\quad \left. \frac{\prod_{t=1}^C \Gamma(\sum_{s=1}^C b_{h_{st}i}^{(st)} + u_{it} + \gamma_i^{(2)}(\epsilon + I(i=t)))}{\Gamma(\sum_{t=1}^C (\sum_{s=1}^C b_{h_{st}i}^{(st)} + u_{it}) + \gamma_i^{(2)}(C\epsilon + 1))} \right) \\ &\propto \sum_{\mathbf{h} \in \mathcal{H}} w_{\mathbf{h}}(\boldsymbol{\gamma}^{(1)}, \boldsymbol{\gamma}^{(2)}, \epsilon) \prod_{i=1}^C p_i^{\sum_{s=1}^C \sum_{t=1}^C b_{h_{st}i}^{(st)} + \delta - 1} \end{aligned}$$

where $w_{\mathbf{h}}(\boldsymbol{\gamma}^{(1)}, \boldsymbol{\gamma}^{(2)}, \epsilon)$ is the weight comprising of all the terms not involving p_i 's. Now, let \mathcal{H}^* denote the subset of \mathcal{H} such that for all $\mathbf{h}^* = (h_{11}^*, h_{12}^*, \dots, h_{CC}^*)' \in \mathcal{H}^*$, each index h_{st}^* corresponds to a partition of v_{st} which allocates v_{st} to the s^{th} partition and zero to all the other partitions. Clearly, for any \mathbf{h}^* , $\sum_{s=1}^C \sum_{t=1}^C b_{h_{st}i}^{(st)} = \sum_{s=1}^C \sum_{t=1}^C v_{st} I(i=s) = \sum_{s=1}^C I(i=s) v_s = v_i$.

Let ζ denote a generic positive constant which does not depend on ϵ and whose value may change from one expression to the next. Noting that $t_{is} = 0$ if $s \neq i$, for any $\mathbf{h}^* \in \mathcal{H}$

and $\mathbf{h} \in \mathcal{H} \setminus \mathcal{H}^*$, we have

$$\lim_{\epsilon \rightarrow 0} \frac{w_{\mathbf{h}}}{w_{\mathbf{h}}^*} = \zeta \prod_{i=1}^C \frac{\prod_{s \neq i} \Gamma(\sum_{t=1}^C b_{h_{st}i}^{(st)} + \gamma_i^{(1)} \epsilon)}{\prod_{s \neq i} \Gamma(\gamma_i^{(1)} \epsilon)} \frac{\prod_{t \neq i} \Gamma(\sum_{s=1}^C b_{h_{st}i}^{(st)} + u_{it} + \gamma_i^{(2)} \epsilon)}{\prod_{t \neq i} \Gamma(\sum_{s=1}^C b_{h_{st}i}^{(st)} + u_{it} + \gamma_i^{(2)} \epsilon)}$$

Since u_{it} 's are greater than zero and there exists at least one pair (i, s) such that $\sum_{t=1}^C b_{h_{st}i}^{(st)} > 0$, the result follows. \square

B Individual cause of death prediction

The calibrated VA is primarily targeted to estimate the CSMF. However, it can also be used to predict the cause of death for each of the individual verbal autopsy reports. The posterior distribution of the true cause of death $G(\mathbf{s}_r)$ of the r^{th} individual is given by

$$\begin{aligned} p(G(\mathbf{s}_r) = i \mid \mathbf{a}, \mathbf{T}) &= \int p(G(\mathbf{s}_r) = i \mid \mathbf{p}, \mathbf{M}, \boldsymbol{\gamma}, \mathbf{a}, \mathbf{T}) p(\mathbf{p}, \mathbf{M}, \boldsymbol{\gamma} \mid \mathbf{T}) dP(\mathbf{M}) dP(\mathbf{p}) dP(\boldsymbol{\gamma}) \\ &= \int p(G(\mathbf{s}_r) = i \mid \mathbf{p}, \mathbf{M}, A(\mathbf{s}_r)) p(\mathbf{p}, \mathbf{M} \mid \mathbf{T}) dP(\mathbf{M}) dP(\mathbf{p}) \\ &= \int \frac{m_{ij} p_i}{\sum_{i=1}^C m_{ij} p_i} p(\mathbf{p}, \mathbf{M} \mid \mathbf{T}) dP(\mathbf{M}) dP(\mathbf{p}) \end{aligned} \quad (12)$$

We can now easily conduct composition sampling using posterior samples of \mathbf{M} and \mathbf{p} to generate a posterior distribution for $G(\mathbf{s}_r)$. This simple application of the Bayes theorem, can recover the individual COD. However, it is a crude approach because the posterior distribution of the COD are identical for all deaths with the same predicted COD from A . Many CCVA algorithms, in addition to providing a predicted COD, also provides the predicted COD distribution for each individual. Utilizing the entire predicted COD distribution from A should lead to improved calibrated estimates of COD. Since estimating individual COD is not the focus of this manuscript, we do not further explore this avenue here.

C Gibbs sampler for ensemble calibration

Let $v_{\mathbf{j}}$ be the number of VA records in the community-wide survey for which algorithm $A^{(1)}$ predicts cause j_1 , $A^{(2)}$ predicts cause j_2 , and so on. Let \mathbf{v}^* be the $C^K \times 1$ vector formed by stacking. Also, let $u_{i\mathbf{j}} = \prod_{k=1}^K m_{ij_k}^{(k)}$ and $\mathbf{u}_{i\mathbf{j}} = (u_{1\mathbf{j}}, u_{2\mathbf{j}}, \dots, u_{C\mathbf{j}})'$.

The posterior $\mathbf{p}, \mathbf{M}^{(1)}, \mathbf{M}^{(2)}, \dots, \mathbf{M}^{(k)}, \gamma^{(1)}, \gamma^{(2)}, \dots, \gamma^{(k)} \mid \mathbf{T}^{(1)}, \mathbf{T}^{(2)}, \dots, \mathbf{T}^{(k)}, \mathbf{q}^*$ is proportional to

$$\prod_{\mathbf{j}} \left(\sum_i u_{i\mathbf{j}} p_i \right)^{v_{\mathbf{j}}} \times \prod_i p_i^{\delta-1} \times \prod_{k=1}^K \left(\prod_{i=1}^C \frac{\Gamma(\gamma_i^{(k)}(C\epsilon + 1))}{(\Gamma(\gamma_i^{(k)}\epsilon))^{C-1} \Gamma(\gamma_i^{(k)}(\epsilon + 1))} \prod_j (m_{ij}^{(k)})^{t_{ij}^{(k)} + \gamma_i^{(k)}(\epsilon + 1(i=j)) - 1} \right).$$

We will once again use data augmentation to implement the Gibbs sampler. Let $\mathbf{b}_{\mathbf{j}} = (b_{1\mathbf{j}}, b_{2\mathbf{j}}, \dots, b_{C\mathbf{j}})'$ denote the $C \times 1$ dimensional realization of a Multinomial $(v_{\mathbf{j}}, \mathbf{1}/C)$ distribution, and let \mathbf{B} denote the $C^K \times C$ matrix formed by stacking the independent $\mathbf{b}_{\mathbf{j}}$'s row-wise for all combinations of \mathbf{j} . Then we have the following full conditionals for the Gibbs sampler:

$$\begin{aligned} \mathbf{b}_{\mathbf{j}} \mid \cdot &\sim \text{Multinomial}(v_{\mathbf{j}}, \frac{1}{\mathbf{1}'(\mathbf{u}_{\mathbf{j}} \odot \mathbf{p})} \mathbf{u}_{\mathbf{j}} \odot \mathbf{p}) \\ \mathbf{M}_{i*}^{(k)} \mid \cdot &\sim \text{Dirichlet} \left(\sum_{\mathbf{j}: j_k=1} b_{i\mathbf{j}} + \gamma_i^{(k)}\epsilon + t_{i1}^{(k)}, \dots, \sum_{\mathbf{j}: j_k=i} b_{i\mathbf{j}} + \gamma_i\epsilon + t_{ii}^{(k)} + \gamma_i, \dots, \sum_{\mathbf{j}: j_k=C} b_{i\mathbf{j}} + \gamma_i\epsilon + t_{iC}^{(k)} \right) \\ \mathbf{p} \mid \cdot &\sim \text{Dirichlet} \left(\sum_{\mathbf{j}} b_{1\mathbf{j}} + \delta, \dots, \sum_{\mathbf{j}} b_{C\mathbf{j}} + \delta \right) \end{aligned}$$

Here \odot denotes the Hadamard (elementwise) product.

Finally, as in Section 3.2, we update $\gamma_i^{(k)}$'s using a metropolis random walk with log-normal proposal to sample from the full conditionals

$$p(\gamma_i^{(k)} \mid \cdot) \propto \frac{\Gamma(C\gamma_i^{(k)}\epsilon + \gamma_i)}{\Gamma(\gamma_i^{(k)}\epsilon)^{C-1} \Gamma(\gamma_i^{(k)}\epsilon + \gamma_i^{(k)})} (\gamma_i^{(k)})^{\alpha-1} \exp(-\beta\gamma_i^{(k)}) \prod_j (m_{ij}^{(k)})^{\gamma_i^{(k)}\epsilon + \gamma_i^{(k)}1(i=j)}$$

C.1 Individual mortality cause predictions

As in Section B, we can predict the individual mortality cause using the ensemble method. Using Bayes theorem we have

$$p(G(\mathbf{s}_r) = i \mid a_r^{(1)} = j_1, \dots, a_r^{(K)} = j_k) = \frac{1}{\sum_{\mathbf{j}} u_{ij} p_i} u_{ij} p_i.$$

Since posterior distributions of u_{ij} 's and \mathbf{p} have already been sampled, we can generate posterior samples of $G(\mathbf{s}_r)$ post-hoc using the composition sampling approach demonstrated in Section B.

For the independent ensemble model, one can recover the posterior distribution of the individual COD in the exact same way. Only additional step would be to first calculate the $\mathbf{u}_{\mathbf{j}}$'s as they are no longer part of the Gibbs sampler.

D Detailed analysis of the simulation results

In this Section we present a much more thorough analysis of the simulation study, as well as investigate additional methods to generate CSMFs for the new country. We first present the exact choices of \mathbf{M} used. We have $\mathbf{M}_1 = \mathbf{I}$,

$$\mathbf{M}_2 = \begin{pmatrix} 1.00 & 0 & 0 & 0 \\ 0.65 & 0.35 & 0 & 0 \\ 0 & 0 & 0.5 & 0.5 \\ 0 & 0 & 0 & 1 \end{pmatrix}$$

and $\mathbf{M}_3 = 0.6 * \mathbf{I} + 0.1 * \mathbf{11}'$. The first choice represents the case where the algorithm A is perfect for predicting COD in the new country. The specific choice of \mathbf{M}_2 depicts the scenario that 65% of Diarrhea/Dysentery cases are classified as Pneumonia and 50% of Sepsis deaths are categorized as some other cause. Finally, \mathbf{M}_3 represents the scenario where there are many small misclassifications.

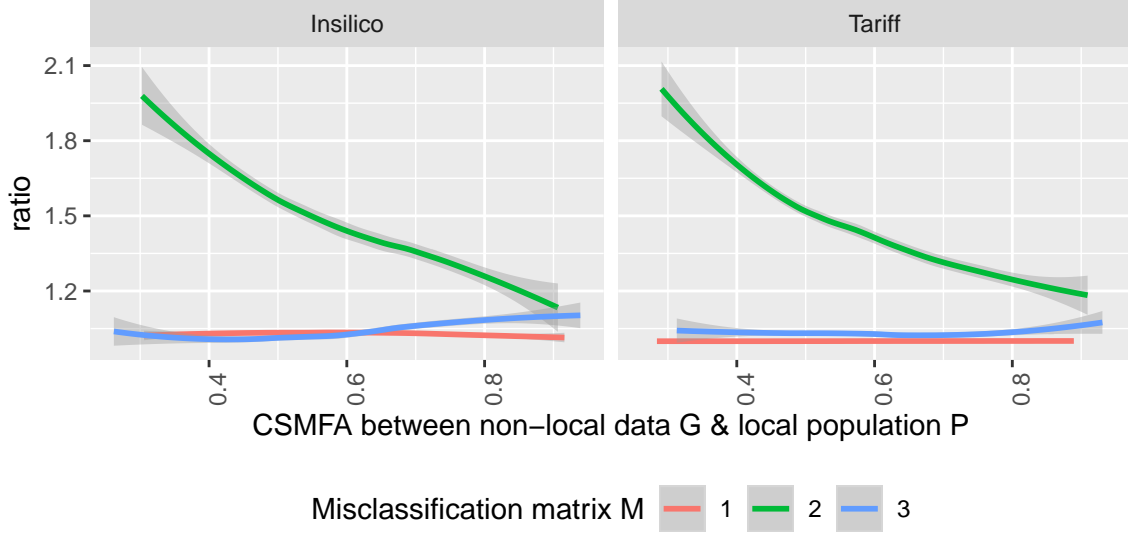


Figure 3: Ratio of CSMFA of calibrated and uncalibrated CCVA

D.1 Disparity in cause distribution between the gold-standard and local data

We first investigate how the performance of calibration is impacted by the disparity in cause distribution between the non-local GS data used to train A and the data in the new country. Figure 3 plots the smoothed ratio of the CSMFA of the calibrated and uncalibrated estimates, as a function of the true CSMFA between the non-local data \mathcal{G} and the local population \mathcal{P} . The left panels correspond to data generated using InsilicoVA and hence assesses the performance of Insilico_G and Insilico_C by plotting the ratio $\text{CSMFA}(\text{Insilico}_C)/\text{CSMFA}(\text{Insilico}_G)$. Similarly, the right panels correspond to data generated using Tariff and compares the estimates from Tariff_G and Tariff_C . We only present the results for $n = 400$, as we will discuss the role of n in Section D.3. We first note that when data was generated using the misclassification matrix $\mathbf{M}_1 = \mathbf{I}$, the ratio is exactly one. This corroborates the result in Theorem 1 that if the CCVA algorithm classifies deaths flawlessly, then the calibrated and uncalibrated CSMF are same. For \mathbf{M}_3 , i.e. when the misclassification rate is small, the ratio

is also close to one with calibrated CSMF being slightly more accurate in general. For \mathbf{M}_2 , which portrays the scenario where the CCVA trained on non-local data is systematically and substantially biased, one can clearly see the benefit of calibration. The calibrated CSMFA is significantly better than the uncalibrated one. It also nicely shows the utility of calibration as a function of x – the CSMFA between the non-local data \mathcal{G} and the local population \mathcal{P} . Unsurprisingly the ratio is decreasing with increasing x . When x is small the ratio is close to two, implying that calibration yields near 100% gain in accuracy. When x is close to one, the improvement is much less stark, which is expected as in this scenario the cause prevalences in the non-local and local populations are almost identical.

D.2 Biases in individual cause prevalences

We also look at the biases in the individual estimates of cause prevalences in Figure 4. The top and bottom rows correspond to data generated using InsilicoVA and Tariff respectively. The three columns correspond to three choices of \mathbf{M} . We see that there is almost no bias for \mathbf{M}_1 for all the methods, for \mathbf{M}_3 the uncalibrated Tariff $_{\mathcal{G}}$ estimates are generally unbiased, whereas the uncalibrated Insilico $_{\mathcal{G}}$ show small biases. However, for \mathbf{M}_2 we see the substantial biases in the estimates from both the uncalibrated approaches. As expected due to the specification of \mathbf{M}_2 , prevalences of Diarrhea/Dysentery and Sepsis are underestimated while those of Pneumonia and Other are overestimated. The calibrated estimates Tariff $_C$ and Insilico $_C$ are unbiased for all the settings.

D.3 Role of the hospital set

We now investigate the role of the sample size n and the CSMF $\mathbf{p}_{\mathcal{H}}$ of the hospital set \mathcal{H} . Additionally, as an alternate to calibration, we also consider including the local GS data \mathcal{H} as part the training data for the CCVA algorithms. So, we have four more methods Tariff $_{\mathcal{H}}$, Tariff $_{\mathcal{G} \cup \mathcal{H}}$, Insilico $_{\mathcal{H}}$ and Insilico $_{\mathcal{G} \cup \mathcal{H}}$, where the sub-script indicates the training data used.

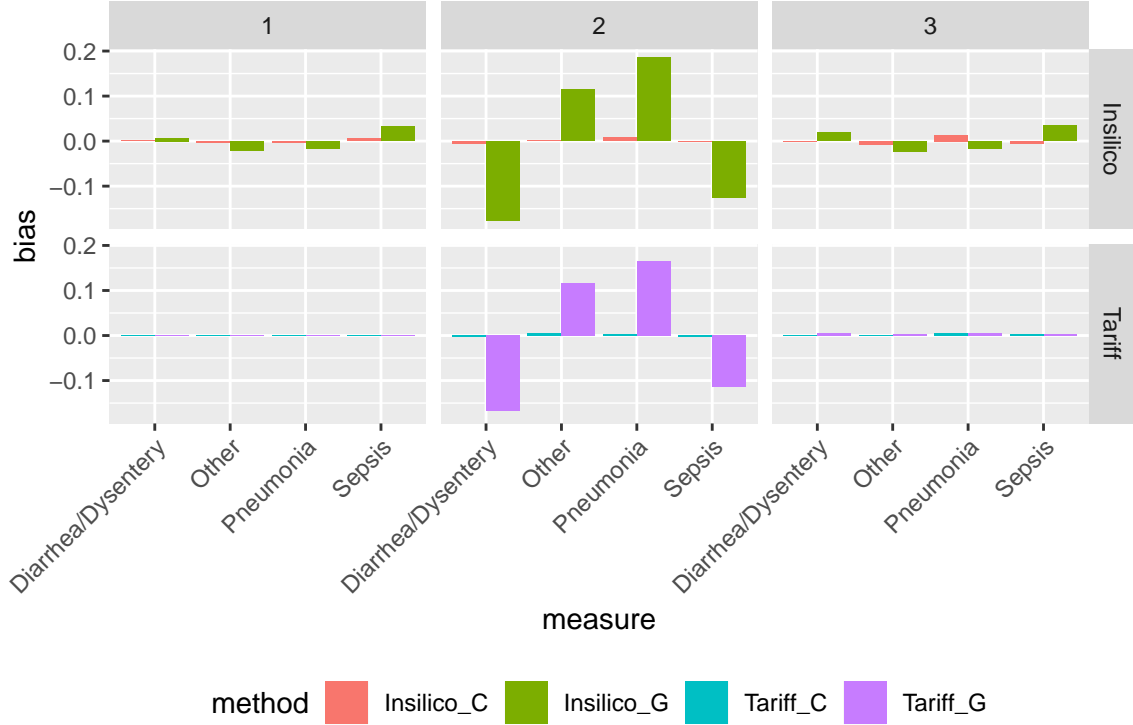
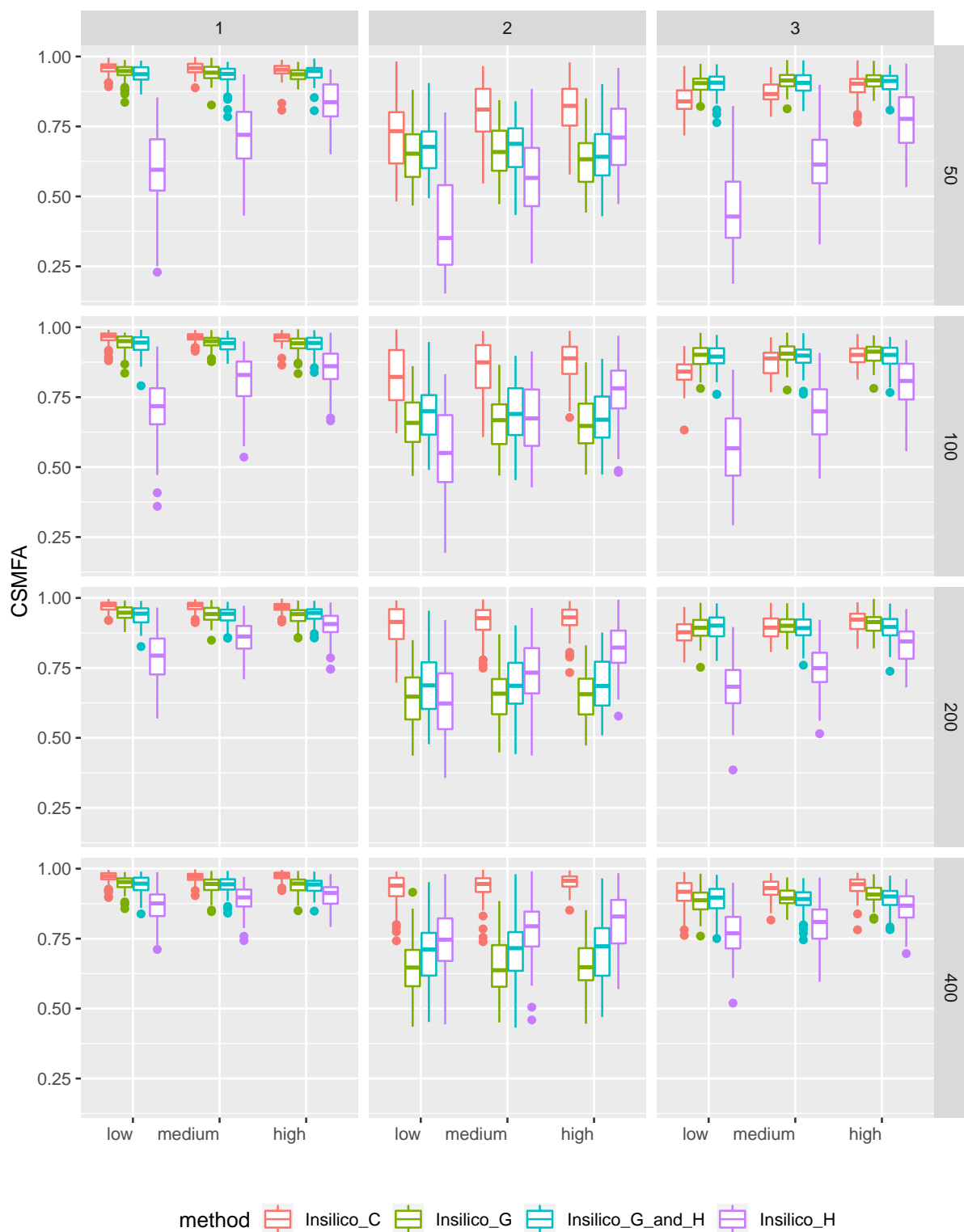


Figure 4: Biases in the average estimates of individual cause prevalences

When data is generated using InsilicoVA, Figure 5 provides the boxplots of CSMF accuracy of the methods for all the scenarios as a function of n (rows), choice of \mathbf{M} (columns) and ρ — the CSMFA-range between $\mathbf{p}_{\mathcal{H}}$ and $\mathbf{p}_{\mathcal{P}}$ (x -axis in each sub-figure). The analogous results for data generated using Tariff, provided in Figure 10 of the supplement, reveals exactly similar trends. We unpack many different conclusions from this Figure. First we look at the performances of Insilico_G and Insilico_C. These two methods was already compared in Section D.1, but only for fixed $n = 400$ and averaged across all $\mathbf{p}_{\mathcal{H}}$. Here, further analyzing the performances as a function of n and ρ , we see that the CSMF of calibrated VA increases with increase in n . Also, there is a drastic gain in precision of the calibrated estimates with the confidence bands shortening with increase in n from 50 to 400. Additionally, we see that the CSMFA for Insilico_C increases as ρ goes from *low* to *medium* to *high*, although the



46
Figure 5: CSMF for additional methods when data is generated using InsilicoVA

gain is not as drastic. This indicates that the calibration procedure, while being reasonably robust to the value of ρ , does benefit to a small extent from improved concordance between the cause prevalences in \mathcal{H} and \mathcal{P} . Of course, $\text{Insilico}_{\mathcal{G}}$ is not affected by either n or ρ . In general, for \mathbf{M}_3 , we see that only when both n is small and ρ is *low*, the $\text{Insilico}_{\mathcal{G}}$ produces slightly better estimates than Insilico_C . For all other cases, Insilico_C yields higher or similar CSMF. For \mathbf{M}_2 , we see Insilico_C dominates $\text{Insilico}_{\mathcal{G}}$ across all scenarios, although the gains from increase in n and ρ are still evident. Finally, for \mathbf{M}_1 , the performance of Insilico_C is identical to $\text{Insilico}_{\mathcal{G}}$, as is guaranteed by Theorem 1, and is not affected by n or ρ .

Next, we look at the performance of $\text{Insilico}_{\mathcal{H}}$ and $\text{Insilico}_{\mathcal{G} \cup \mathcal{H}}$. For \mathbf{M}_1 and \mathbf{M}_3 , $\text{Insilico}_{\mathcal{H}}$ performs quite poorly, generally producing the lowest CSMF. $\text{Insilico}_{\mathcal{H}}$ is also highly sensitive to both ρ and n , yielding highly variable and inaccurate estimates for *low* ρ and n , and improving sharply as either increases. Only for \mathbf{M}_2 , for large n or large ρ , it does better than $\text{Insilico}_{\mathcal{G}}$. As this setting portrays substantial difference in the symptom-cause dynamics between the non-local and local population, $\text{Insilico}_{\mathcal{H}}$, trained on local data, does better. CSMF from $\text{Insilico}_{\mathcal{G} \cup \mathcal{H}}$, which uses both the local and the non-local GS data in the training, generally lies between the CSMF from $\text{Insilico}_{\mathcal{G}}$ and $\text{Insilico}_{\mathcal{H}}$, and is much closer to the former as the non-local GS data far outnumbers the local data. Finally, comparing $\text{Insilico}_{\mathcal{H}}$ and $\text{Insilico}_{\mathcal{G} \cup \mathcal{H}}$ to Insilico_C , we see that the latter does substantially better uniformly across the scenarios. This shows that with a small hospital set, our calibration approach is a more resourceful way of exploiting this limited data and results in more accurate and robust estimates.

D.4 Comparison with the naive calibration

To understand the importance of the Bayesian regularization used in the calibration, we also compare with the naive calibration based on MLE, outlined in Section 3. Like its Bayesian analog, the naive calibration method works with the output of a CCVA algorithm. We

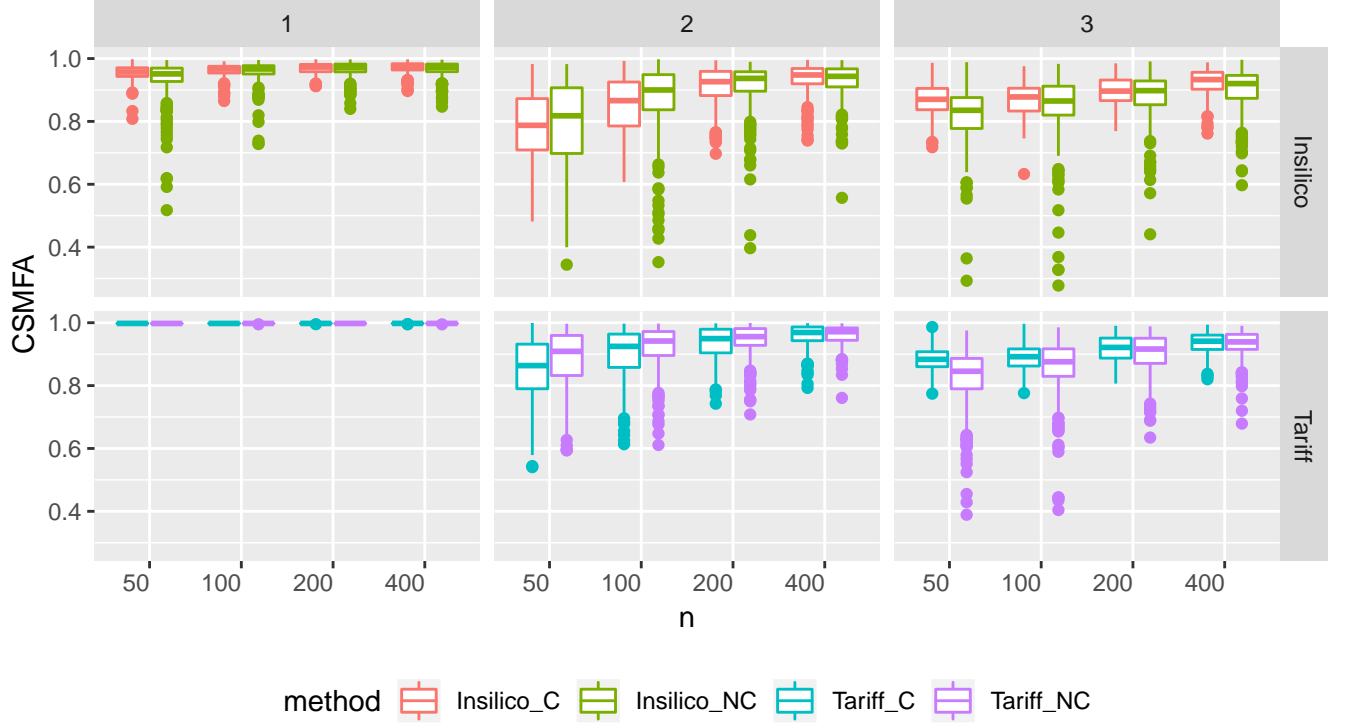


Figure 6: CSMF of naive and Bayesian calibration

refer to the naive calibration methods using Tariff and InsilicoVA respectively as Tariff_{NC} and Insilico_{NC} . Figure 6 compares the CSMFA for the naive and Bayesian calibration approaches. Once again, the top and bottom row corresponds to data generated using Tariff and InsilicoVA respectively, the three columns are for three choices of \mathbf{M} and within each setting, we plot the boxplots of CSMF as a function of n .

We see that, generally the median estimates from the naive calibration is similar to the ones produced using the Bayesian regularized calibration. However, there is notable difference in the variation of CSMF estimates produced, with the naive calibration producing a wide range of values with several extreme estimates. The problem is exacerbated for smaller values of n . The results from the Bayesian model are more stable with uniformly lesser variation across all the settings. It is evident, that in real data analysis, where the

truth is unknown, the Bayesian model will be much more reliable than the naive calibration which seems to be quite likely to yield absurd estimates.

D.5 Performance of ensemble calibration

We now analyze the performance of the joint (Ensemble_J) and independent (Ensemble_I) ensemble calibration models introduced in Section 4. These models use output from both Tariff and InsilicoVA whereas the individual calibration models Tariff_C and Insilico_C which only use the output from one CCVA algorithm. For a given dataset, we define

$$\delta = \max(\text{CSMFA}(\text{Insilico}_C), \text{CSMFA}(\text{Tariff}_C)) - \min(\text{CSMFA}(\text{Insilico}_C), \text{CSMFA}(\text{Tariff}_C)).$$

In other words, δ denotes the difference in CSMFA of the calibrated VA using the most and least accurate CCVA algorithms. When δ is small, both algorithms are performing in a similar way, whereas larger values of δ clearly insinuate that one of the CCVA algorithm is more accurate than the other in estimating the population CSMF. For an ensemble method that aims to guard against inclusion of an inaccurate method, one would expect that CSMFA for the ensemble method should be closer to that of the best performing method. Equivalently, if

$$\nu = \text{CSMFA}(\text{Ensemble}) - \min(\text{CSMFA}(\text{Insilico}_C), \text{CSMFA}(\text{Tariff}_C)),$$

where Ensemble refers to either Ensemble_I or Ensemble_J , then ν should be greater than $\delta/2$.

Figure 7 plots ν as a smoothed function of δ . We first note that, for \mathbf{M}_1 (red lines), the curve for the joint sampler nearly coincides with the 45-degree line. Since, in our data generation process, under \mathbf{M}_1 one of the CCVA algorithms is fully accurate, this empirically verifies the theoretical guarantee in Theorem 2, that in such settings CSMF estimate from the ensemble calibration is same as that from the best individual calibration. While the independent ensemble model does not enjoy this theoretical property, in practice we see that for \mathbf{M}_1 , ν is also identical to δ . For \mathbf{M}_2 and \mathbf{M}_3 , across all scenarios, ν is close to

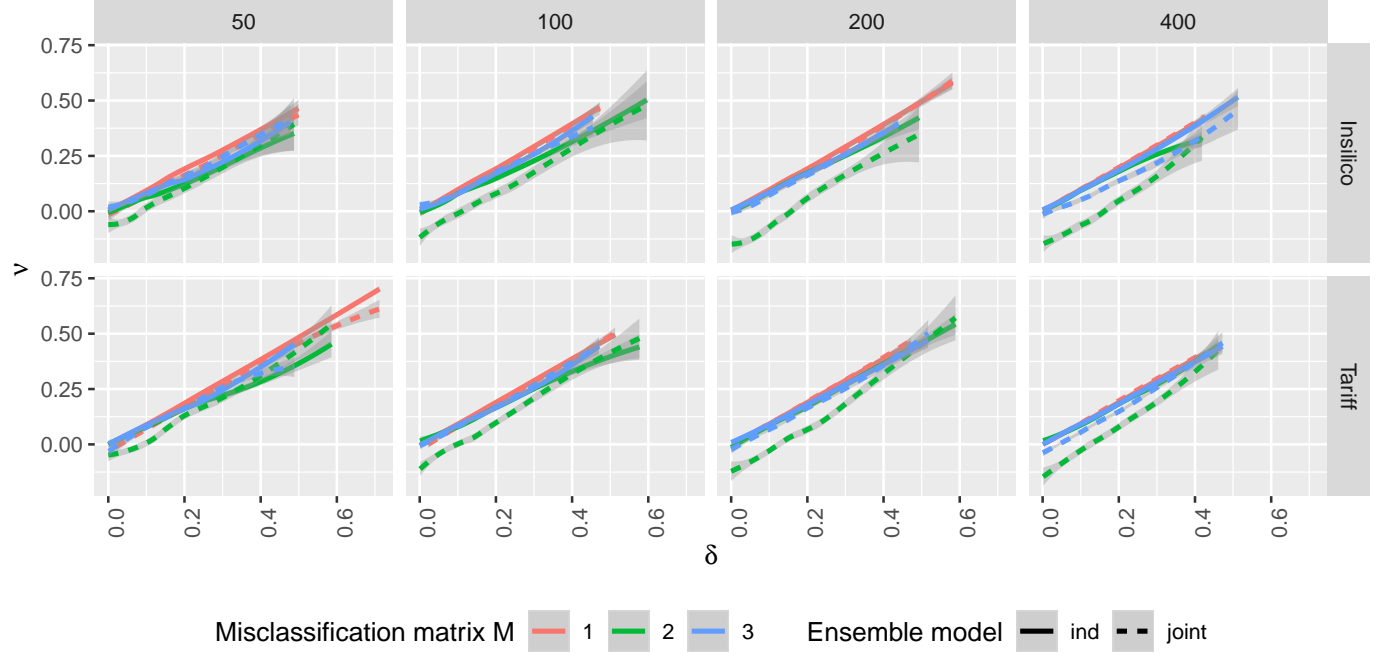


Figure 7: Performance of the ensemble calibration models

δ , i.e. CSMF estimates from both the Ensemble_J and Ensemble_I models generally aligns much closer to the best performing individual calibration model. There are no significant trends with respect to either the size of \mathcal{H} (n) or the data generating CCVA algorithm – Insilico (top-row) and Tariff (bottom-row). The Ensemble_I model seems to do slightly better than the joint model. Since, it is also the faster model, we only use this version of the ensemble calibration for subsequent analysis. The performance of the ensemble samplers is quite reassuring especially for larger δ , as it demonstrates the robustness to inclusion of a bad method via averaging over multiple methods. As ν seems to be substantially greater than $\delta/2$ for most of the curves, it also shows why our model based method averaging is superior to simply taking average of the estimated CSMF from the different methods which is much more affected by the worst method. More detailed boxplots for the CSMF of each

of the methods are provided in Figures 9 and 1 in the Supplement.

D.6 Individual COD predictions

As mentioned earlier, prediction individual CCC is not our primary goal. Nonetheless, we have outlined a way to obtain calibrated individual COD predictions and here we compared its accuracy using the Chance Corrected Concordance (Murray, Lozano, Flaxman, Vahdatpour & Lopez 2011) defined as

$$\text{CCC} = \frac{1}{C} \sum_{i=1}^C \frac{\frac{TP_i}{TP_i+TN_i} - \frac{1}{N}}{1 - \frac{1}{N}}$$

where TP_i and TN_i denote the true positive and true negative rates for cause i . We only analyze the case when the data is generated using Insilico (Figure 11). The roles are simply reversed when data is generated using Tariff (Figure 12). We see in Figure 11 that CCC for Insilico $_G$ and Insilico $_C$ are better than those of Tariff $_G$ and Tariff $_C$ respectively. This is expected as analyzing data using the true model is expected to perform better than the misspecified model. CCC from the calibrated (Insilico $_C$) and uncalibrated (Insilico $_G$) versions of the same CCVA algorithm, which was used in data generation, were similar. For the misspecified model, the calibrated CCVA (Tariff $_C$) produced slightly better CCC than its uncalibrated analog (Tariff $_G$). However, these gains in CCC from calibration are not substantial and perhaps indicates that if individual COD prediction is of interest then more advanced methods need to be considered than the simple approach we have adopted. However, even using our crude approach, we see that the ensemble calibration (Ensemble $_I$) produces CCC closer to Insilico $_C$ and Insilico $_G$, and much better than the CCC obtained by both Tariff $_C$ and Tariff $_G$. This once again furnishes evidence of the robust performance of the ensemble model, and in practice, when we will not know which CCVA algorithm works best, using the ensemble model will safeguard against choosing a bad VA algorithm.

E Sensitivity analysis for India and Tanzania

We employed a resampling approach similar to (Murray, Lopez, Black, Ahuja, Ali, Baqui, Dandona, Dantzer, Das & Dhingra 2011) in order to perform a sensitivity analysis of whether the (empirically determined) specific CSMFs of the training set $\mathbf{p}_{\mathcal{G}}$ and population set $\mathbf{p}_{\mathcal{P}}$ in the PHMRC data led to the superior performance of the calibrated VA for the data analysis in Section 6. To sample data into \mathcal{G} and \mathcal{P} , we drew $\mathbf{p}_{\mathcal{G}}$ and $\mathbf{p}_{\mathcal{P}}$ (both of length $K + 1$) from independent uninformative Dirichlet distributions. We sampled 800 subjects from outside of the country of interest, with replacement according to probability $\mathbf{p}_{\mathcal{G}}$ and based on their GS-COD, into \mathcal{G} . A similar process was used to create \mathcal{P} , except using records from exclusively within the country of interest and using the probability vector $\mathbf{p}_{\mathcal{P}}$. For creating \mathcal{H} , we sampled n subjects from within the country of interest with replacement, using the empirical distribution of COD within that country. We used \mathcal{G} to train models $Tariff_{\mathcal{G}}$, $Insilico_{\mathcal{G}}$ and calibrated them using \mathcal{H} to get $Tariff_C$, $Insilico_C$, and $Ensemble_I$. We used the $\mathbf{p}_{\mathcal{P}}$ drawn from the Dirichlet distribution as the true CSMF and computed the CSMFA for all the models. This whole process was repeated 500 times for each country, value of K , and value of n .

We again can visualize the results for $K = 7$ in Figure 8. First observation is that the CSMFA of all algorithms is dramatically lower than in Section 6 and have higher uncertainty. This is expected as we are now averaging over 500 pairs of difference cause distributions for the training and test set. In general most of the trends revealed in Section 6 persist here although the differences are more moderate. We do see that the calibrated methods $Tariff_C$ and $Insilico_C$ perform better than the uncalibrated analogs $Tariff_{\mathcal{G}}$ and $Insilico_{\mathcal{G}}$ respectively, with the gain in CSMFA becoming more substantial with increase in n . However, now that the size of \mathcal{P} stays constant at 800, we see an increase in CSMFA as n increases for all three calibration models. The improvement of CSMFA with respect to n is most dramatic as n changes from 100 to 200 for $Tariff_C$. It appears that $Ensemble_I$ generally performs slightly

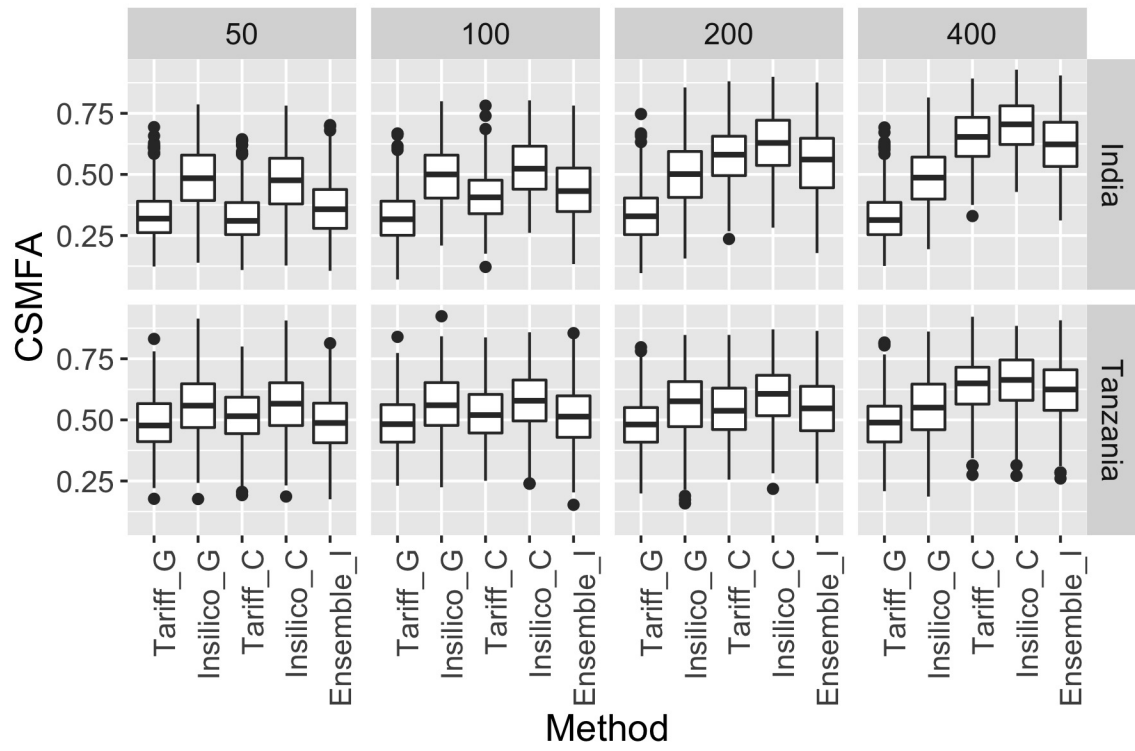


Figure 8: Sensitivity analysis of CSMFA of competing algorithms for the top 7 COD + others

worse for smaller sample sizes but benefits from an increase in n . Overall, the sensitivity analysis shows that over a large range of possible CSMF compositions for \mathcal{G} and \mathcal{P} , calibrated VA performs well in predicting $\mathbf{p}_{\mathcal{P}}$.

We also repeat the analysis in Section 6 and the sensitivity analysis using the top 3 causes plus *Other* instead of the top 7 plus *Other* causes. The results are presented in Figures 13 and 14. Most trends presented for the top 7 causes are also present here. The only difference is that the Ensemble_I method generally performs much better in case, aligning closely with the more accurate CCVA algorithm for most of the scenarios.

E.1 Additional figures

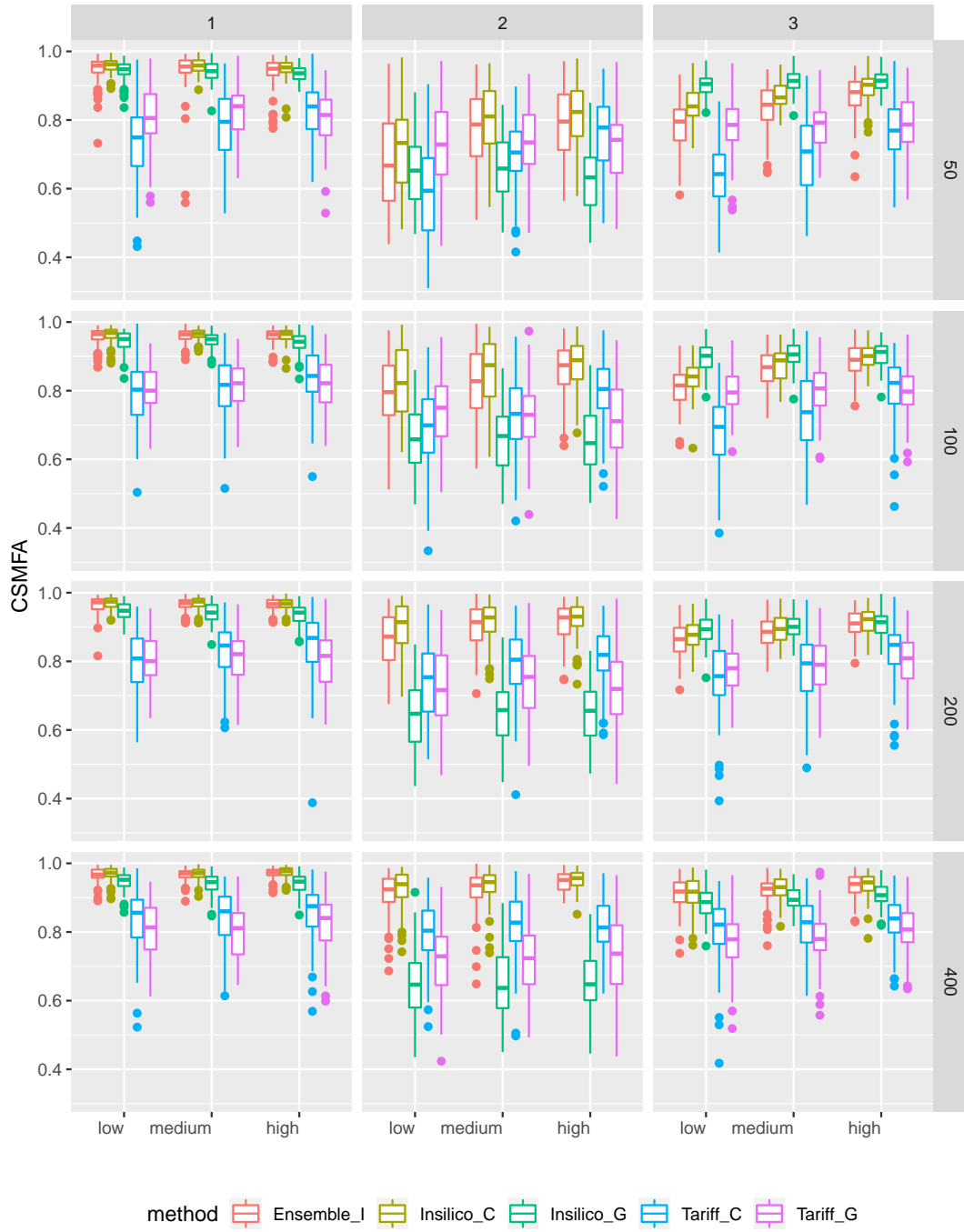


Figure 9: CSMF when data is generated using InsilicoVA

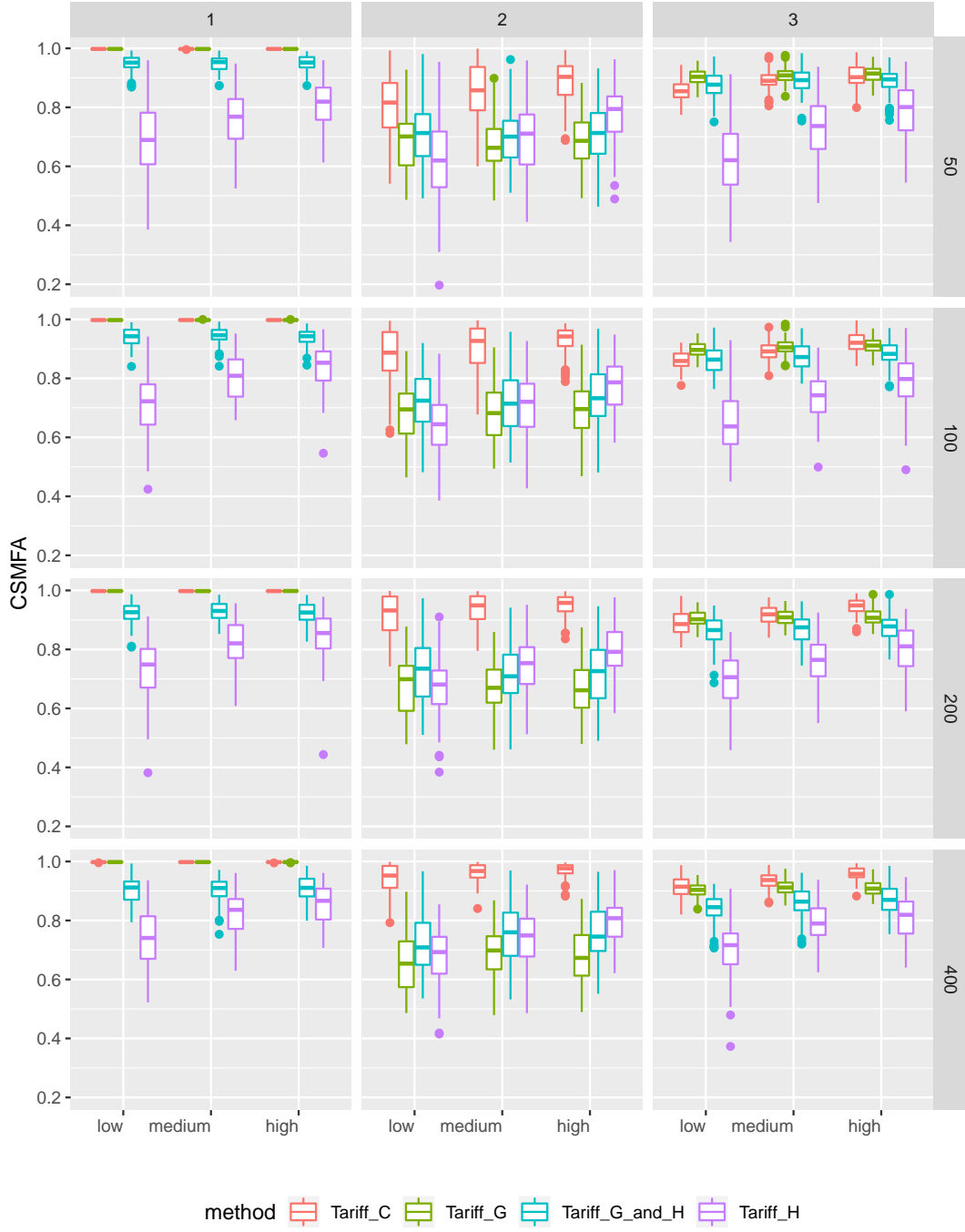


Figure 10: CSMF for the additional methods of Section D.3 when data is generated using Tariff

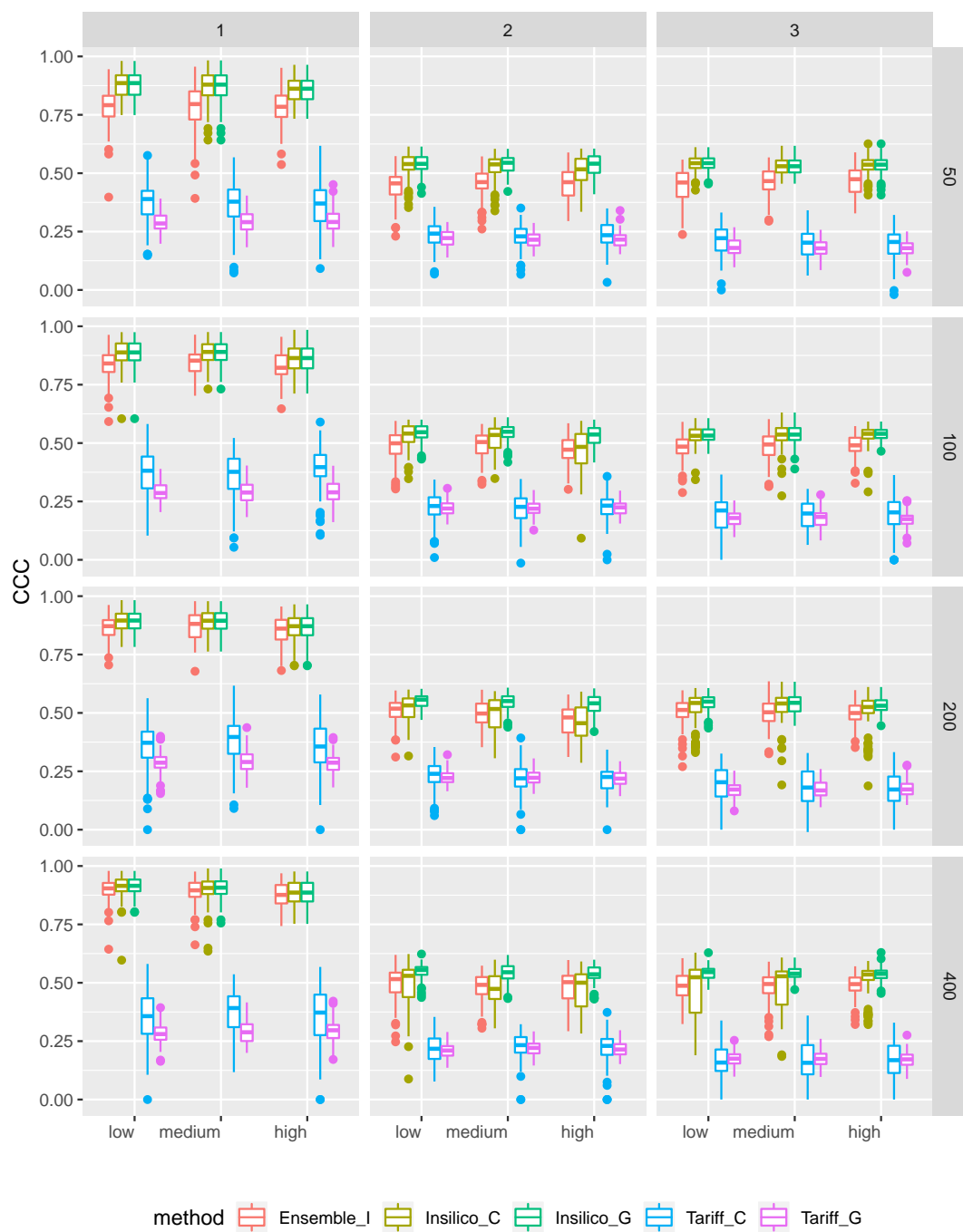


Figure 11: CCC when data is generated using InsilicoVA

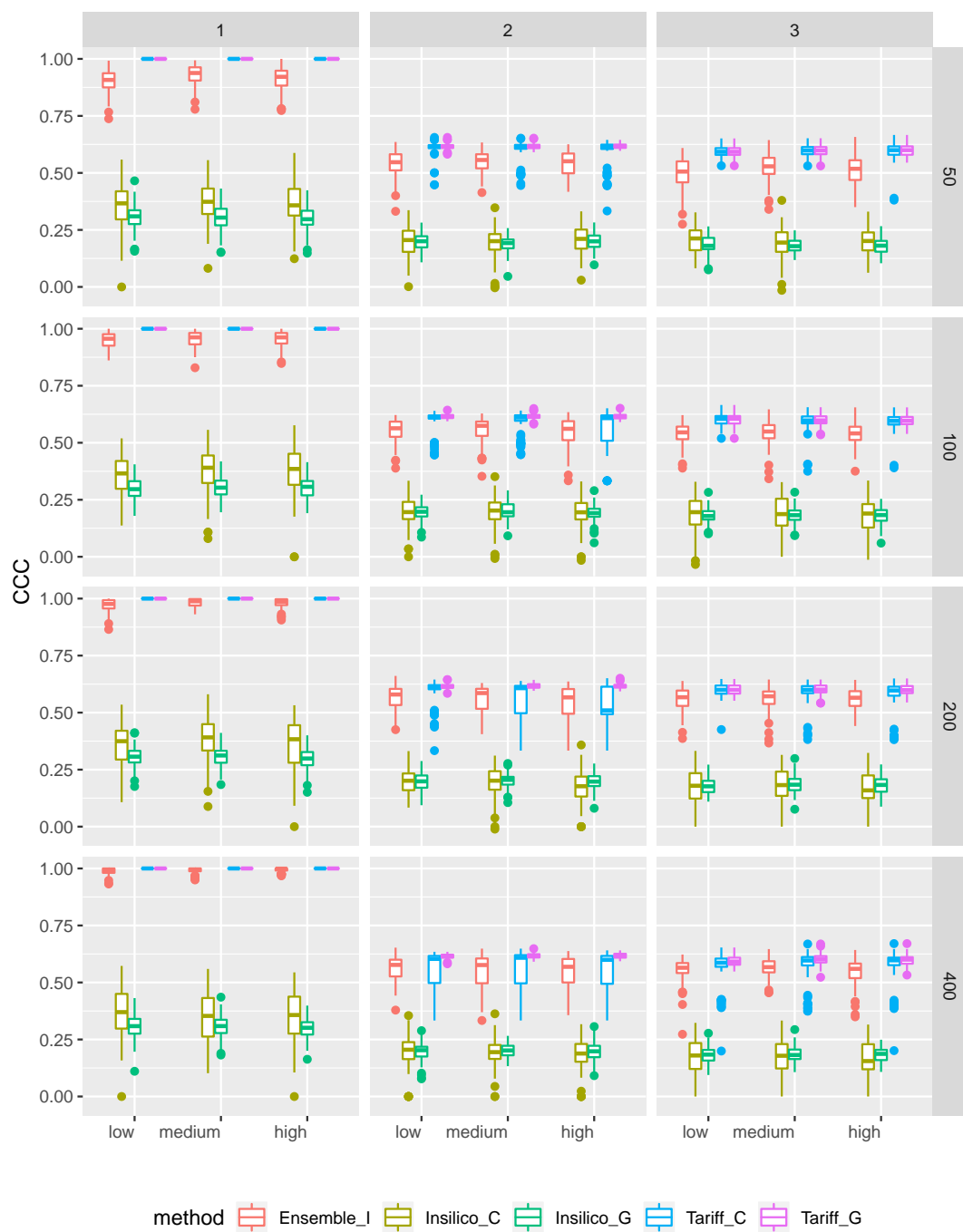


Figure 12: CCC when data is generated using Tariff

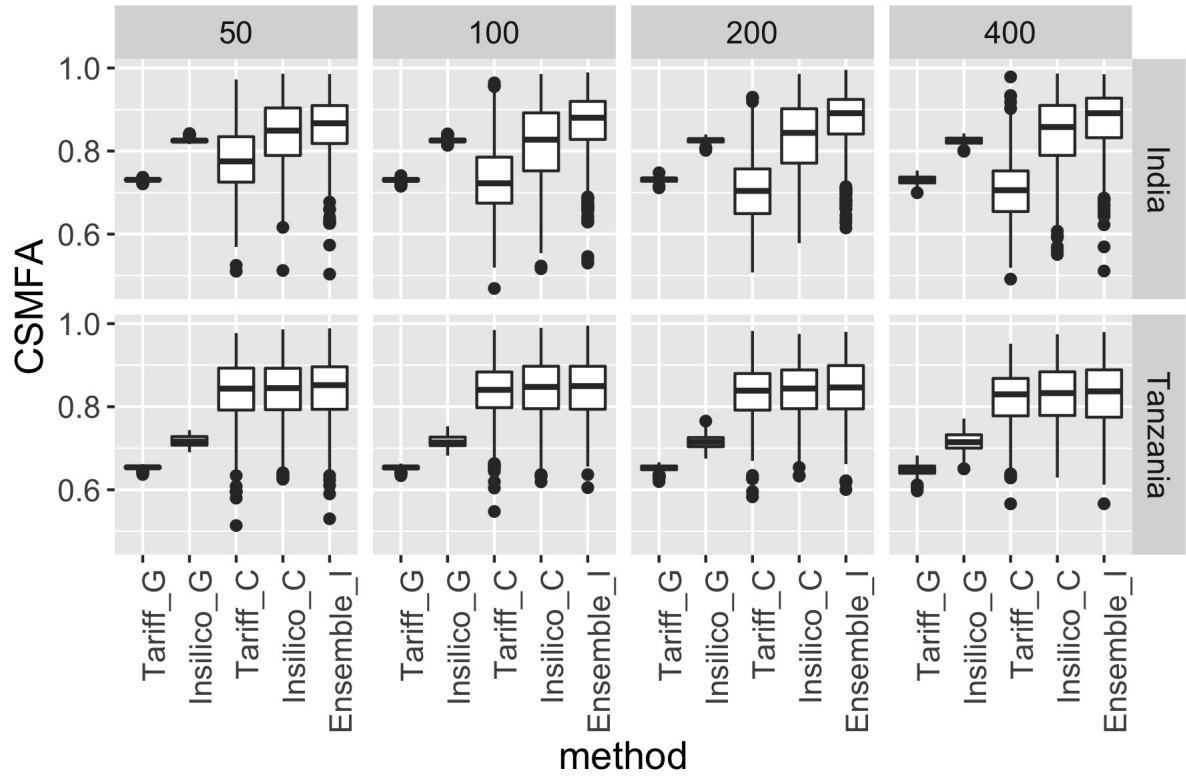


Figure 13: CSMFA of competing algorithms using true GS-COD labels for the top 3 COD + others

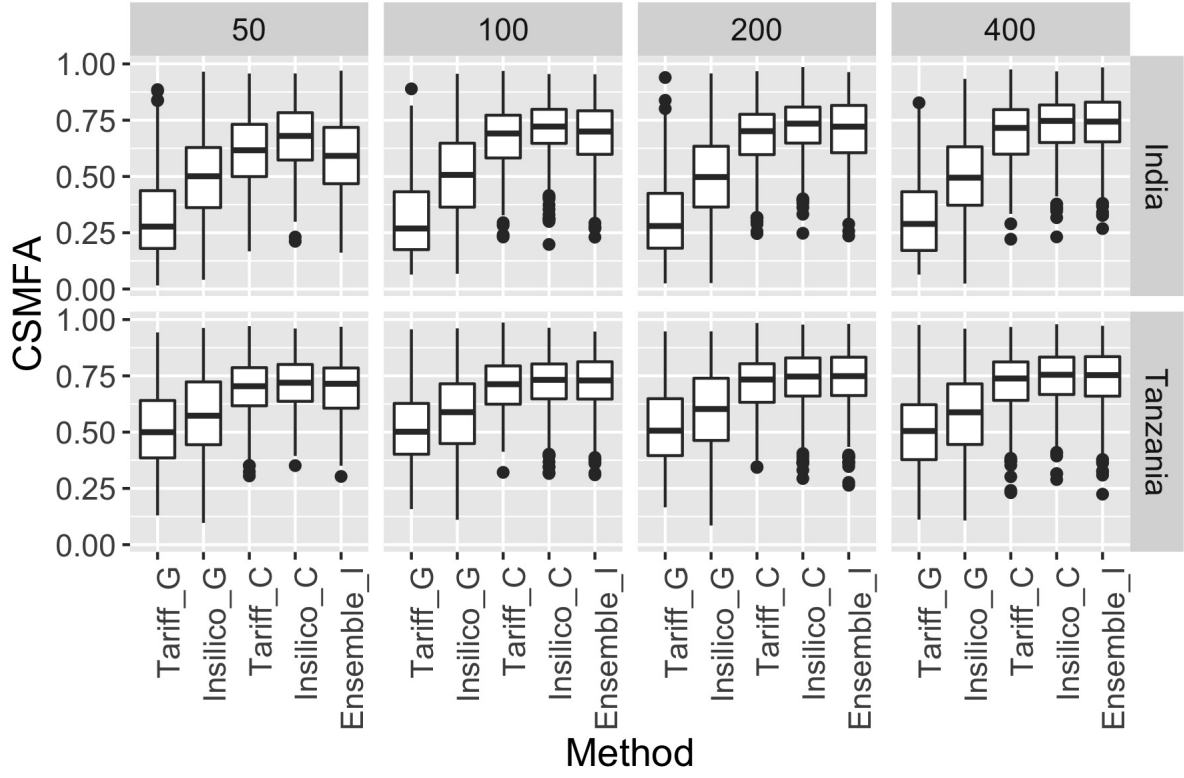


Figure 14: Sensitivity analysis of CSMFA of competing algorithms for the top 3 COD + others